การเก็บกลับคืนแร่ธาตุหายากจากหลอดฟลูออเรสเซนต์ที่หมดอายุใช้งานแล้ว

นางสาวชรริน ลิ่มตระกูล

วิทยานิพนธ์นี้เป็นส่วนหนึ่งของการศึกษาตามหลักสูตรปริญญาวิศวกรรมศาสตรมหาบัณฑิต
สาขาวิชาวิศวกรรมทรัพยากรธรณี ภาควิชาวิศวกรรมเหมืองแร่และปิโตรเลียม
คณะวิศวกรรมศาสตร์ จุฬาลงกรณ์มหาวิทยาลัย
ปีการศึกษา 2554

RECOVERY OF RARE EARTH ELEMENTS FROM END OF LIFE FLUORESCENT LAMP

Miss Chorarin Limtrakul

A Thesis Submitted in Partial Fulfillment of the Requirements

for the Degree of Master of Engineering Program in Georesources Engineering

Department of Mining and Petroleum Engineering

Faculty of Engineering

Chulalongkorn University

Academic Year 2011

Thesis Title	RECOVERY OF RARE EARTH ELEMENTS FROM END OF LIFE FLUORESCENT LAMP
By	Miss Chorarin Limtrakul
Field of Study	Georesources Engineering
Thesis Advisor	Associate Professor Quanchai Leepowpanth, Ph.D.
Thesis Co-advisor	Associate Professor Dawan Wiwattanadate, Ph.D.

Accepted by the Faculty of Engineering, Chulalongkorn University in Partial Fulfillment of the Requirements for the Master's Degree

…….. Dean of the Faculty of Engineering
(Associate Professor Boonsom Lerdhirunwong, Dr.Ing.)

THESIS COMMITTEE

…….Chairman
(Associate Professor Pinyo Meechumna, Ph.D.)

…….Thesis Advisor
(Associate Professor Quanchai Leepowpanth, Ph.D.)

…….Thesis Co-advisor
(Associate Professor Dawan Wiwattanadate, Ph.D.)

…….External Examiner
(Assistant Professor Teanchai Tonthai, Ph.D.)

ชรวิน ลิ่มตระกูล : การเก็บกลับคืนแร่ธาตุหายากจากหลอดฟลูออเรสเซนต์ที่หมดอายุใช้งานแล้ว. (RECOVERY OF RARE EARTH ELEMENTS FROM END OF LIFE FLUORESCENT LAMP) อ. ที่ปรึกษาวิทยานิพนธ์หลัก : รศ.ดร. ขวัญชัย ลีเผ่าพันธุ์, อ. ที่ปรึกษาวิทยานิพนธ์ร่วม รศ.ดร. ดาวัลย์ วิวรรธนะเดช, 109 หน้า.

หลอดไฟฟลูออเรสเซนต์เป็นหลอดไฟที่ปล่อยประจุอิเล็กตรอนผ่านไอปรอท หลอดไฟฟลูออเรสเซนต์ถูกนำมาใช้โดยทั่วไปหรือในตึกสูง เนื่องจากมีประสิทธิภาพสูงกว่าหลอดไฟทั่วๆไป อย่างไรก็ตามองค์กรสิ่งแวดล้อมของประเทศสหรัฐอเมริกาได้ระบุคัดแยกหลอดไฟฟลูออเรสเซนต์ให้เป็นขยะมีพิษ และแนะนำให้คัดแยกขยะเพื่อนำกลับมาใช้ใหม่หรือกำจัดให้ปลอดภัย นอกจากนั้นส่วนประกอบหลักของสารเคลือบหลอดไฟฟอสฟอร์ยังมีแร่ธาตุหายากผสมอยู่ เช่น La (แลนทานัม), Tb (ทริปเบียม), Ce (ซีเซียม), Eu (ยูโรเปียม) และ Y (ยิบเตียม) ซึ่งมีราคาสูง ดังนั้นหลอดไฟฟลูออเรสเซนต์ที่ผ่านการใช้งานแล้วจึงถูกนำมาพิจารณาถึงแหล่งของทรัพยากรทุติยภูมิของแร่ธาตุหายาก

ในการศึกษาวิจัยครั้งนี้ การใช้ตะแกรงแบบแห้งโดยใช้การสั่นและคลื่นอัลตร้าโซนิกได้ถูกนำมาวิเคราะห์ในการคัดแยกแร่ธาตุหายาก จากฟอสฟอร์ในหลอดไฟฟลูออเรสเซนต์ที่ผ่านการใช้งานแล้ว ฟอสฟอร์ที่ยังไม่ผ่านการใช้งานจะนำมาวิเคราะห์หาคุณลักษณะ เช่น การกระจายตัวของอนุภาค, ความถ่วงจำเพาะ, ส่วนผสมของฟอสฟอร์แต่ละสี ก่อนที่จะทำการทดลอง การใช้ตะแกรงสั่นด้วยคลื่นอัลตร้าโซนิก 5, 8, 10 และ 12.5 ด้วยเวลา 2 นาทีถูกนำมาคำนวณหาขนาดตะแกรงที่ดีที่สุด และการใช้ตะแกรงสั่นด้วยน้ำถูกนำมาทดสอบเพื่อเปรียบเทียบกับการใช้ตะแกรงแบบแห้ง ในการเก็บกลับคืนแร่ธาตุหายาก อิทธิพลของขนาดตะแกรงและเวลาถูกนำมาวิเคราะห์เพื่อจะหาค่าที่ดีที่สุดในการคัดแยก การคัดแยกด้วยกระแสอากาศเพื่อเป็นการทดสอบประสิทธิภาพของการคัดแยก และหาค่าที่ดีที่สุดในการป้อนตัวอย่าง 10 kg/h ด้วยความเร็ว 2000, 3000, 4000, 5000, 6000 and 7000 rpm ที่มีพัดลมอัดอากาศและไม่มีพัดลมอัดอากาศ

ภาควิชา..วิศวกรรมเหมืองแร่และปิโตรเลียม..ลายมือชื่อนิสิต ……
สาขาวิชา…....วิศวกรรมทรัพยากรธรณี..... ลายมือชื่อ อ.ที่ปรึกษาวิทยานิพนธ์หลัก……
ปีการศึกษา……..…..2554……ลายมือชื่อ อ.ที่ปรึกษาวิทยานิพนธ์ร่วม ……

5270263821 : MAJOR GEORESROUCES ENGINEERING

KEYWORDS : RARE EARTH ELEMENT / ULTRASONIC SIEVING / WET SIEVING / DRY SIEVING/ AIR CLASSIFICATION / RECYCLING

CHORARIN LIMTRAKUL : RECOVERY OF RARE EARTH ELEMENTS FROM END OF LIFE FLUORESCENT LAMP. THESIS ADVISOR : ASSOC. PROF. QUANCHAI LEEPOWPANTH, Ph.D., THESSIS CO-ADVISOR ASSOC.PROF. DAWAN WIWATTANADATE, Ph.D., 109 pp.

Fluorescent lamp is a gas-discharge lamp that uses electricity to excite mercury vapor. However, the United States Environmental Protection Agency classifies fluorescent lamps as hazardous waste, and recommends that they are segregated from general waste for recycling or safe disposal. In addition, main components of fluorescent lamp are rare earth phosphor including La (Lanthanum), Tb (Terbium), Ce (Cerium), Eu (Europium) and Y (Yttrium), the price of which has become increasing. Therefore, the used fluorescent lamps are considered as an important secondary resource for rare earth element.

In this study, ultrasonic dry sieving as well as wet vibration sieving has been used for separation of rare earth elements from the ground used lamp. Sample characterization then separation, tests were conducted. Ultrasonic dry sieving in 5, 8, 10 and 12.5 μm for 2 minutes each was performed to determine the optimum sieve size, and then wet vibration sieving 5 μm was conducted in different times to compare wet and dry sieving. In the recovery of rare earth elements process, influences of sieving size and time were investigated in order to identify the optimum condition for the separation process. In term of the air classification which is an instrument to verify the separation performance of dry separation process, the optimum condition was obtained when the feed rate is 10 kg/h with rotation speed of 2000, 3000, 4000, 5000, 6000 and 7000 rpm by with and without compressed air.

Department : Mining and Petroleum Engineering Student's Signature .....

Field of Study : Georesources Engineering Advisor's Signature .....

Academic Year : 2011 Co-advisor's Signature .....

ACKNOWLEDGEMENTS

Foremost, I would like to thank my thesis advisor, Assoc. Prof. Dr. Quanchai Leepowpanth, who shared with me a lot of his expertise and research insight. I would also like to express my gratitude to my thesis co-advisor, Assoc. Prof. Dr. Dawan Wiwattanadate, for kind suggestion on the issues during I was Japan.

It is difficult to overstate my appreciation to Asst. Prof. Dr. Pinyo Meechumna and Prof. Dr. Tsuyoshi Hirajima, who gave me valuable advice and assistant on the application for Friendship Scholarship.

This study has been progressed due to series of dialogues with my Japanese advisor, Prof. Dr. Keiko Sasaki, and also Mr. Masayuki Kuwata, Master degree at the same department in Kyushu University. Through their thoughtful and wise questioning, it brought me closer to the reality I had initially perceived, eventually enabling me to grasp its rich complexity.

I am deeply grateful to Kyushu University for providing Friendship Scholarship to fund this thesis.

I am indebted to Toshiba Company and Jeiriraitsu Company, Kitakyushu for providing spent automobile catalytic converters in this study.

Sincere thanks are expressed to thesis committee members, Asst. Prof. Dr. Teanchai Tonthai from the Department of Chemical Engineering, for their kind and applicable suggestions.

Many thanks are extended to all members in the Department of Mining and Petroleum Engineering, whose friendship and support are beyond a place of study.

I am forever grateful to my father who stay in my mind and my mother who has always supported and encouraged me to do my best in all matters of life. Particular thanks, of course, to my younger sister and brother, who keep me up when I feel discourage.

The author alone assumes responsibility for the conclusions of this thesis and any errors it may contain.

CONTENTS

LIST OF TABLES

LIST OF FIGURES

FIGURE PAGE

FIGURES PAGE

CHAPTER I

INTRODUCTION

1.1 General Introduction

In 1999, the US Environmental Protection Agency (EPA) added a provision for mercury-containing lamps to the Universal Waste Rule (UWR). Universal wastes are hazardous waste items commonly disposed by households and small businesses in the solid waste stream. The UWR was developed to encourage recycling and proper disposal of these wastes, which meet the Federal criteria for hazardous waste but are widely generated and typically do not pose an immediate and undue risk. Universal wastes are subject to less stringent standards for handling, storage, and transport. Full hazardous waste requirements remain, however, for the final recycling, treatment or disposal of these wastes. Specific UWR requirements vary based on the volume of universal waste handled or generated, so generators are encouraged to review the rule and seek additional information as needed from the US EPA and their local and state authorities (Litex Industries et al., 2009)

Lighting accounts for approximately 20% of electricity use in commercial buildings. Energy-efficient commercial lighting products currently on the market present a variety of opportunities for reducing electricity consumption and lowering electric utility costs for office buildings, retail and wholesale stores, schools, public buildings, and factories. While energy efficient fluorescent (including compact fluorescent) and high intensity discharge (HID) lamps - metal halide lamps used primarily in warehouses, sports facilities, parking lots, tall buildings and stores, and mercury vapor lamps used in street lighting - have long been a staple in schools, public, commercial, industrial buildings, and roadways, replacing those lamps with more efficient fluorescent and HID lamps, lighting controls, and electronic ballasts can lower electricity consumption and reduce electricity costs significantly (Litex Industries et al., 2009).

Fluorescent lamps use 25%-35% of the energy used by incandescent lamps to provide the same amount of illumination. HID lamps use 10-25% of the lighting energy of incandescent lamps they replace. The comparative energy-efficiency of fluorescent lamps and HID lamps is made possible because an electric arc converts a tiny amount of mercury in the lamp to a gas, which enables the creation of visible light. Mercury is the only known element that will provide the energy-efficiency experienced by fluorescent and metal halide lamps. Ultraviolet lamps used in tanning equipment and for germicidal purposes as well as neon lamps also use small amounts of mercury. At the end of a fluorescent, ultraviolet, neon, or metal halide lamp's life, there is an even smaller amount of mercury gas left in the tube and mercury atoms that still adhere to the interior of the lamp (Litex Industries et al., 2009).

To keep the small amount of remaining mercury in a spent lamp out of landfills, businesses, schools, governments and building owners should dispose of fluorescent, ultraviolet, neon, and metal halide lamps separately from regular commercial and building waste. Some states mandate that businesses and building owners recycle mercury-added lamps. Local waste disposal and public works authorities should be consulted for lamp recycling requirements and opportunities. An entire industry of commercial lamp recyclers[6] has evolved to collect and recycle fluorescent and HID lamps from apartment and office buildings, retail stores and warehouses, schools and government buildings.[7] This website provides businesses and building owners with an opportunity to find commercial lamp recyclers in their area (Litex Industries et al., 2009).

Lighting manufacturers, through their trade association, National Electrical Manufacturers Association (NEMA) developed lamprecycle.org to provide a one-stop source of information about recycling lamps (the term used in the lighting industry to refer to all types of light bulbs). Compact fluorescent lamps (CFLs), and with other energy-efficient lighting such as linear fluorescent and high intensity discharge (HID) lamps contain a very small amount of mercury, an element essential to achieving energy

savings. While these lamps help consumers and businesses cut their lighting energy usage and reduce energy costs, it is important that any product containing mercury be properly managed when it becomes waste to protect public health and the environment. Easy and convenient options exist for both businesses and consumers to recycle waste mercury-containing lamps. It is estimated that businesses already recycle over 30% of their waste lamps annually and consumers are embracing lamp recycling as they switch to more efficient lighting technologies (Litex Industries et al., 2009).

Figure 1.1 Fluorescent Lamp

In Oct. 2010, the Chinese has announced plans to cut production and slash exports of the materials in (Rare Earth Metals, 2011). From the fact that more than 95% of the world's rare earth output comes from China, the shortage of REE supply seemed to be worse. Up to date, the demand for REE is still higher while the supply is lower. A growing supply/demand imbalance is resulting in a higher REE price (see Figure 1.1) that already affects lamp manufacturers' cost and finally to the selling prices of the end products.

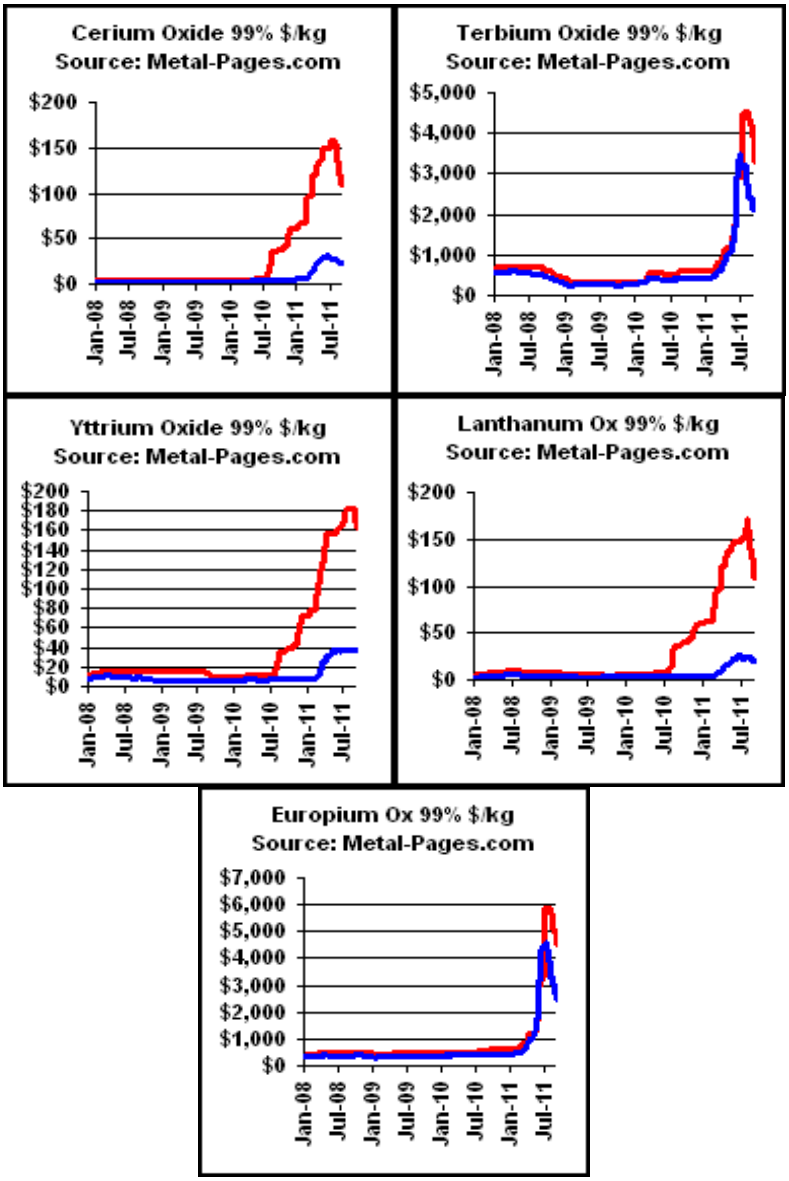

Figure 1.1 Prices of rear earth oxides in Chinese market: red line-FOB index; blue line-in China.

To overcome the shortage of REE supply, new source of REE is still required. Nowadays, the used fluorescent tube as a kind of industrial waste is considered to be a potential urban mining resource for the recovery of rare earth metals through recycling

(Hirajima et al., 2005; Rabah, 2004). Although the recycling ratio of waste fluorescent lamps accounts only for approximately 10% of the Japanese production (Nishisu et al, 2004), the disposed waste is a potential source of rare earth elements that can be recovered to supply an industry that largely relies on the foreign market (Hirajima et al, 2005).

In this study, used fluorescent lamps were characterized and relationships between REE in samples and the quantity of phosphors were investigated. Calibration curves were created to predict amount of REE in those used samples. Then, various separation methods were employed in order to separate REE from used fluorescent lamp and the quantity of REE was estimated using the developed calibration curves. Finally, Newton's efficiency of each separation method was evaluated.

1.2 Objectives

To study physical separation of rare earth element phosphor from used phosphor base on size and density to develop environmental friendly method and to find an optimum condition that can be practically used to recover REE from used fluorescent lamp.

1.3 Scopes

1. To characterize fresh and used fluorescent lamps in order to quantify the amount of REE in used fluorescent lamps. The characterization included:
    a) elemental analysis using X-ray fluorescent (XRF)
    b) particle size distribution using a laser scattering analyzer
    c) determination of specific gravity using a density measuring device

d) morphology investigation using a Scanning Electron Microscope with Energy Dispersive X-ray (SEM-EDX)

2. To find optimum conditions of three physical separation methods used to recover REE from used fluorescent lamp. The separation methods were: a) dry sieving (vibration and ultrasonic sieving), b) wet sieving, and c) air classifier.

3. To evaluate the recovery rates of REE using aforementioned separation methods at optimum conditions.

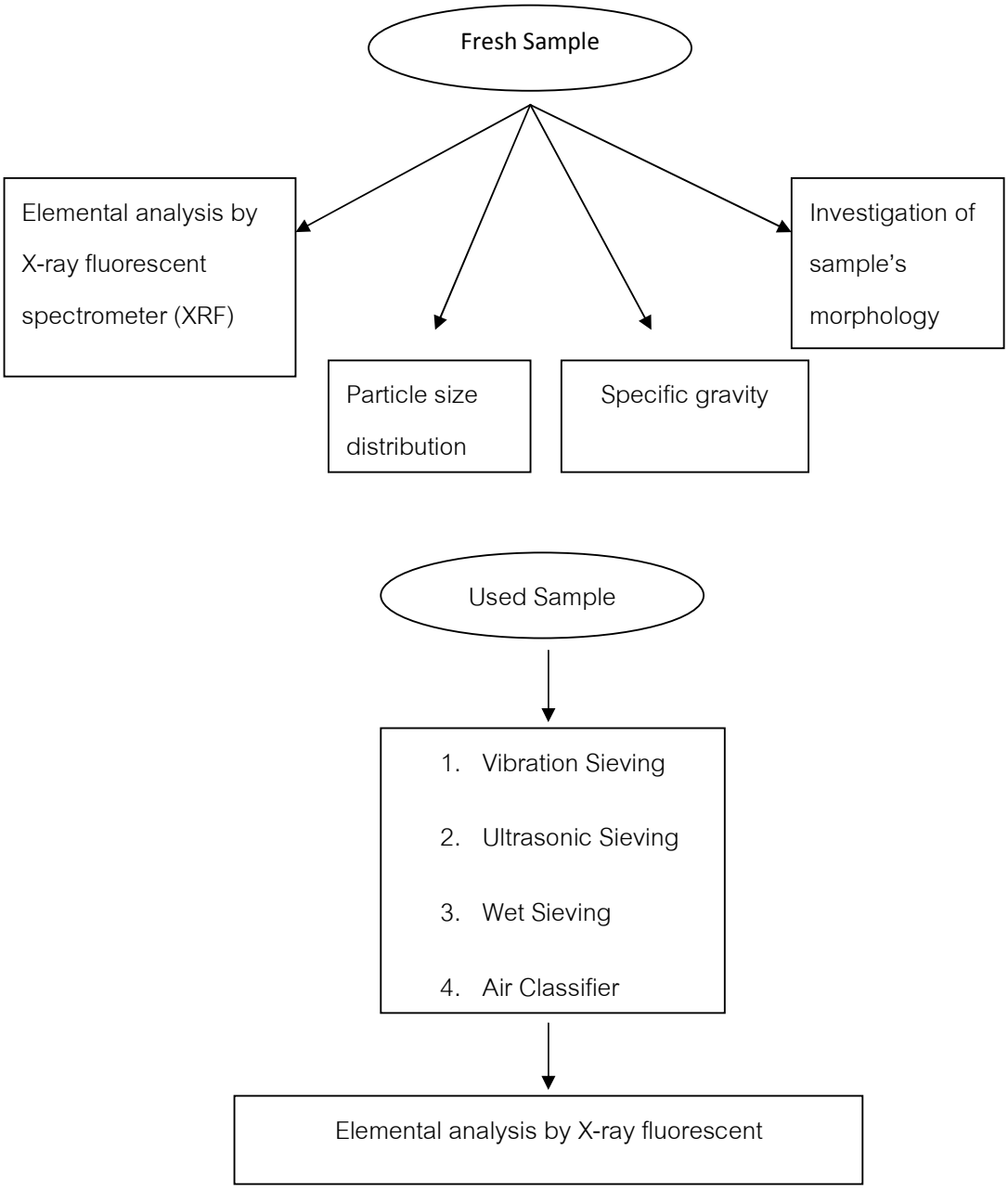

Figure 1.2 Schematic flowchart of the present study

1.4 Expected benefits

It was expected that a new environmental friendly, cost-saving and effective method was developed from this study. The developed method was also supposed to be practical for industrial use to recover REE from used fluorescent lamps.

1.5 Order of presentation

In order to present this research and make it easy to understand for readers, the author has divided this research into these 4 chapters;

Chapter 1 Introduction: General introduction, objectives of the study, outlines of the study and expected benefits.

Chapter 2 Backgrounds and literatures reviews

Chapter 3 Characterization of samples: Introduction, experimental, results and discussion, conclusion.

Chapter 3 Separation of Rare Earth Oxides: Vibration sieving, Ultrasonic Sieving, Wet sieving and Air Classifier.

Chapter 4 Conclusion: Conclusion, recommendation and suggestion.

CHAPTER II

BACKGROUNDS AND LITERATURE REVIEWS

2.1 The Importance of rare earth elements

In the quest for a more efficient lighting system, lighting industry has undergone considerable improvement with the advent of tri-chromatic rare earth phosphors (or rare earth element - REE) for the production of fluorescent tubes. At the end of the life cycle of fluorescent tubes, these newly introduced materials have usually been discarded, after mercury removal, together with traditional calcium halo-phosphate phosphors as waste products. Residues generated through this process are either discarded as special waste, or subjected to a cost-intensive chemical process aimed at extracting the finely ground particles of phosphors (Shimuzu et al., 2005).

REE comprises about 85% of phosphors that can be used in the production of fluorescent lamps. Besides lighting industry, REE is essential to the operation of a variety of products which includes flat-panel displays, color TVs, medical devices, the batteries used in hybrid and electric vehicles, and catalytic converters. REE can also be used in some processes like petroleum refining and so on (Shimuzu et al., 2005).

2.2 Description of rare earth elements

There are 17 rare earth elements (REEs), 15 within the chemical group called lanthanides, plus yttrium and scandium. The lanthanides consist of the following: lanthanum, cerium, praseodymium, neodymium, promethium, samarium, europium, gadolinium, terbium, dysprosium, holmium, erbium, thulium, ytterbium, and lutetium. Rare earths are moderately abundant in the earth's crust, some even more abundant than copper, lead, gold, and platinum. While some are more abundant than many other minerals, most REEs are not concentrated enough to make them easily exploitable economically. The United States was once self-reliant in domestically produced REEs, but over the past 15 years has become 100% reliant on imports, primarily from China, because of lower-cost operations.

2.3 Recovery and Recycle of fluorescent lamp

Workers can prevent exposure, save money disposing of higher-cost broken lamps, and prevent breakage by storing lamps safely. Among the storage options:

- Put used lamps in original boxes, with no packing material. Make sure to completely seal the box to prevent leaks from bulb breakage. When combining used lamps with new ones, mark the used with a piece of tape or a permanent marker, and make sure tape or a marker is located next to the receptacle.

- Buy specially made lamp containers for storing used lamps. These containers often are reusable and durable, and they won't tip over easily. Lamp recyclers might have a container that they like to use to make shipping or pick-up easier.

Also, workers should never leave spent lamps unattended or in a compromising position, such as leaning against a wall or in an area where they can be easily broken. They shouldn't tape lamps together, and they should store boxes and containers in a dry place. If possible, they should stack boxes and containers neatly on pallets and shrink-wrap them. Clearly identify containers of used lamps. For example, label the container used fluorescent lamps for recycling and include the accumulation start date.

Some states still allow certain low-mercury fluorescent lamps to be landfilled, but managers should avoid this practice, as even small amounts of mercury can have a significant impact. All mercury-containing fluorescent lamps should be sent for recycling.

2.4 Literature and reviews

T.Hirajima studies about Zeta-potential measurements were made to determine the electric state of phosphor materials on the basis of which a feasibility study could be performed for the use of flotation in the recovery of fine (d_{50}<13 μm) rare earth phosphors from waste fluorescent lamps. Tests were carried out with pure specimens of white (calcium halo phosphate), red, green and blue (rare earth) phosphors, with a 17:1:1:1 ratio of their mixture, and with actual waste phosphor materials. The effects of a cationic (dodecyl ammonium acetate, DAA) and two anionic (sodium dodecyl sulfate (SDS) and sodium oleate (NaOl)) collectors on the floatability of materials, as well as that of Na_2SiO_3 dispersant on the separation characteristics, were investigated at different pH ranges. The process, applied to actual discarded waste phosphors gave, in a two-stage separation scheme, sink products assaying 17.7–23.8% and 21.5–25.9% rare earth phosphors for DAA and SDS flotation, respectively. The recovery and Newton's

efficiency were about 70–90% and 0.26–0.37, 66–82% and 0.18–0.20, respectively for DAA and SDS flotation.

T.Hirajima studies about the experiments were carried out with waste phosphors collected during the recycling of end-of-life fluorescent lamps to obtain a highly enriched phosphors product as starting material for the better extraction of rare earth elements. The aim of this work was therefore to separate low-density calcium halo-phosphate phosphors from high-density rare earth-activated phosphors through dense-medium centrifugation (with di-iodomethane as organic dense-medium). The feasibility of the process and the conditions for a good separation (higher Newton's efficiency) appear to be a function of the rotation speed of the centrifugal separator, the pulp concentration and the adsorption of a surfactant (sodiumoleate, NaOl) during the pre-treatment stage. The effect of the centrifugation time was less pronounced. Through this study, a sink product assaying 48.61% of rare earth-activated phosphors could be recovered from waste phosphor materials pre-treated with 5×10^{-5} mol/dm^3 of sodium oleate (NaOl) surfactant. The Newton's efficiency and recovery of the separation were 0.84 and 97.34%, respectively. The process feasibility was reinforced by the possibility to recover, through laboratory batch tests, more than 99.8% of the di-iodomethane (CH_2I_2).

Mahmound A. Rabah studies about Europium and Yttrium metals and some valuable salts were recovered from the powder coating the inner surface of the glass tubes of fluorescent lamps. The tubes were broken under 30% aqueous acetone to avoid emission of mercury vapor to the atmosphere, and the powder was collected by brushing. Metals available in the powder were pressure leached using sulfuric/nitric acid mixture. Sulphate salt of europium and yttrium so obtained was converted to thiocyanate. Trimethyl-benzylammonium chloride solvent was used to selectively extract Eu and Y from the thiocyanate solution. The metal loaded in the organic solvent was

recovered by N-tributylphosphate in 1 M nitric acid to produce nitrate salts of Eu and Y. Europium nitrate was separated from yttrium nitrate by dissolving in ethyl alcohol. The isolated powder contained 1.62% europium oxide, 1.65% yttrium oxide, 34.48% calcium sulphate, 61.52% Ca orthophosphate and 0.65% other impurity metals by weight. Autoclave digestion of the powder in the acid mixture for 4 h at 125 °C and 5 MPa dissolved 96.4% of the yttrium and 92.8% of the europium. Conversion of the sulphate to thiocyanate is favoured at low temperature. Extraction of Eu and Y from the thiocyanate solution attained its maximum at 80 °C. N-tributylphosphate in 1 N nitric acid at 125 °C achieved a stripping extent of 99%. Thermal reduction using hydrogen gas at 850 °C and 1575 °C produced europium and yttrium metals, respectively. A metal separation factor of 9.4 was achieved. Economic estimation revealed that the suggested method seemed feasible for industrial applications.

W. S. Hall and J. K. Beddowl study about a major phenomenon that lowers the efficiency of conventional sieving processes is an effect known as ‘blinding’. When blinding occurs, particles tend to block up and lodge in the sieving mesh and it has been demonstrated that the process of blinding in batch sieving is a transient one and occurs in four distinct stages. Also, it has been reported recently that the value of the residual or hard blinding is strongly affected by both particle size and particle shape.

KeShun Liu studies about compared the two methods for sieving performance and efficiency using flours made from soft white and hard white wheat, hulless barley and medium grain rice. Additional factors, including milling method (impact vs. abrasive), flour moisture (7% vs. 11%), duration of sieving (60 vs. 120 min), and tapping (percussion during sieving), were also investigated. Mass frequency and protein content of oversize fractions were measured. Results show that all the variables and their interactions had significant effects on sieving performance and efficiency. Among them, tapping was most important, followed by sieving duration, sieving method, milling

method, flour type, and flour moisture. When other conditions were equal, the reverse sieve method always gave improved sieving efficiency over the stacked sieve method. The observation can be attributed to the beneficial effect of oversized particles on reducing sieve blinding by near or sub-sieve sized particles. Furthermore, the reverse sieve method also expanded the difference in protein content among sieved fractions. Because of its practical significance, this so far unreported effect would bear further confirmation of other sieving and screening conditions.

Lijie GuoTurbo studies about the air classifier are one of the most widely used powder classification equipment. The rotor cage as a rotary component can create a forced centrifugal field, so it is a key part for turbo air classifier. In order to investigate the effect of structural variations of the rotor cage on flow field characteristics, three dimensional velocity measurements of the annular region in a turbo air classifier equipped with two different rotor cage bottom plates (A and B type) are performed by laser Doppler velocimeter (LDV). It is found that the different bottom plates have different axial and tangential velocity distributions in the annular region. However, the structural variations of the rotor cage have hardly any effect on the radial velocity. Based on the classification principle, the relation between the classification performance and the flow field characteristics is investigated in great detail. The results of the flow field measurements were tested by the classification experiments carried out with cement raw meal and ground calcium carbonate. The results demonstrate that B type bottom plate can realize the production of narrow particle size distributions, so it is more favorable for classification than A type bottom plate. Classification experiment results are in good agreement with the results of the flow field measurements.

CHAPTER III

CHARACTERIZATION OF SAMPLES

3.1 Introduction

Although sieving/screening has played important roles in studying and processing particulate materials, it has not received enough scientific attention (Leschonski et al., 1979). Simplicity and familiarity of the process may explain this curious situation. In reality, sieving process is governed by multidisciplinary principles, ranging from physics to applied fluid mechanics. It has been identified that key factors that affect this unit operation include the size and shape of particles relative to the aperture of the sieve, the mesh size of the sieve itself, the amount of material on the sieve surface, the movement direction of the sieve and the rate of movement of material relative to the sieve surface (Liu et al., 2009). Furthermore, the size distribution of particulate matter is very important in determining its physicochemical properties in a large number of processes of various industries (e.g. production of food powders, chemicals, colorants, paints, and pharmaceuticals) (Liu et al., 2009). Thus characterization of the sample is an important step that should be investigated for an effective sieving process.

In this chapter, characterization of samples used in this experiment which included white, red, blue and green phosphors were extensively reported. Firstly, quantitative analysis of elements in sample was performed using an X-ray fluorescent spectrometer (XRF). Then, particle size distribution was evaluated using a laser scattering particle size distribution analyzer while particle shape were investigated by a

mean of scanning electron microscopy. Lastly, specific gravity (SG) was determined using a densitometer.

It should be mentioned here that in this report red, blue and green phosphors are called rare earth phosphors while the impurities referred to white phosphor and glass.

3.2 Experimental

3.2.1 Materials

There were two types of sample used in this experiment: fresh and used samples (from used fluorescent lamps recycling plant). The former was obtained from Toshiba Company while the latter from Jeiriraitsu Company, Kitakyushu.

Since the used sample generally contained metal, mercury, glass and phosphor, the pre-seperation process was applied to try to purify the sample as much as possible. Metal and mercury were eliminated from the bulk using magnetic and distillation process. Then sample was mixed with water. Glass was physically separated from the floating portion on water surface while used phosphor which was heavier than water was collected from the bottom. Dry glass and phosphor were finally obtained after drying wet samples in an oven.

Figure 3.1 Fresh samples in 325 μm wave length light (white, red, blue and green phosphor)

Figure 3.2 Appearance of used phosphor

3.2.2 Elemental analysis by X-ray fluorescent spectrometer (XRF)

In this experiment, the fresh samples were obtained from Toshiba Company and the used sample by recycle of fluorescent lamps was obtained from Jeiriraitsu, Kitakyushu. Samples were pulverized in the mortar for 30 min and compressed into pallets. An X-ray fluorescent spectrometer (Primus RIGAKU, Japan) was used to perform elemental analysis.

To investigate the effect of mercury content in the used samples on the composition of the used samples, mercury-free samples and sample that still contained mercury were both analyzed.

3.2.3 Particle size distribution

In this experiment the particle size distribution of fresh samples (white, red, blue and green phosphor) were analyzed. The samples were firstly mixed with 0.02%w/v sodium hydroxide solution in order to dispersed particles to the final concentration of 100 g/L before measured for its size distribution using a laser scattering analyzer (HORIBA LA-950, Japan). The reflective indexes (RI) of white, red, blue and green phosphors used in the calculation are 1.63, 1.82, 1.58 and 1.962 respectively.

3.2.4 Specific gravity

Known amount of fresh samples (white, red, blue and green phosphor) were measured for their volumes by a mean of helium replacing in a density measuring device (Pycnomatic, Japan) under vacuum condition. The volume of the sample was determined from the volume of helium used and the specific gravity was finally calculated from net volume and mass of sample.

3.2.5 Investigation of sample's morphology

To accurately and precisely evaluate sample's morphology, a Scanning Electron Microscope with Energy Dispersive X-ray (SEM-EDX, Japan) was employed to image the shapes of particles at various magnification ranged from x500 to x4000.

3.3 Results and discussion

3.3.1 Elemental analysis

Table 3.1 shows the main elements in fresh white, red, blue and green phosphor and used glass which was obtained from sedimentation in water. Shortly, CaO (57.6%) and P_2O_5 (39.5%) were found to be the main elements presented in white phosphor. Green phosphor consisted of 57.6% La_2O_3, 19.8% CeO_2 and 10.7% Tb_4O_7. Red phosphor was found to contain mainly Y_2O_3 (92.17%) and only few amount of Eu_2O_3 (7.59%). In contrast only 0.0272% Y_2O_3 was found in blue phosphor. For glass sample the main component was SiO_2 (72.6 wt%) as expected. Our results were well agreed with the simplified formulas proposed by Hirajima et al. (2005) (see Table 3.2). It was also found that the quantity of oxide of each element in fresh samples was similar with those in the used sample.

Table 3.1 Compositions of white, red, green, blue phosphors and *glass (from used sample)

White phosphor		Green phosphor		Red phosphor		Blue phosphor		*Glass	
Element	%wt	Element	%wt	Element	%wt	Element	%wt	Element	%wt
CaO	57.600	La_2O_3	42.900	Y_2O_3	92.1700	Al_2O_3	70.900	SiO_2	72.600
P_2O_5	39.500	P_2O_5	25.600	Eu_2O_3	7.5900	BaO	18.700	Na_2O_3	12.800
MnO	1.570	CeO_2	19.800	Al_2O_3	0.0261	Eu_2O_3	5.450	CaO	7.510
Sb_2O_3	0.565	Tb_4O_7	10.700	SiO_2	0.1650	MgO	4.610	MgO	3.170
Cl	0.484	MgO	0.681	CaO	0.0891	SiO_2	0.221	Al_2O_3	2.010
SiO_2	0.237	SiO_2	0.194	SO_3	0.0047	NaO_2	0.112	K_2O	1.450
Al_2O_3	0.057	Al_2O_3	0.148			P_2O_5	0.038	Sb_2O_3	0.142
SrO	0.023					Y_2O_3	0.027	Fe_2O_3	0.132
SO_3	0.017							Cl	0.066
								P_2O_5	0.030
								ZnO	0.017
								SrO	0.013
								ZrO2	0.013
								SO_3	0.009

Table 3.2 Simplified formula of each phosphor (Hirajima et al., 2005)

Phosphor Materials	Simplified formula
White	$3Ca_3(PO_4)_2.Ca(F,Cl)_2$:Sb,Mn
Red	$(Y,Eu)_2O_3$
Blue	$(Sr, Ca, Ba, Eu)_{10}(PO_4)_6.Cl_2$
Green	$(La, Ce, Tb)(P,B)O_4$

Since mass ratio of elements in white, red, blue and green phosphor were different, thus it was possible to relate mass ratio of each phosphor with the amount of elements found in the bulk. For example, if there is a used sample that contained unknown amount of rare earth and impurities but the main element in this sample was found to be CaO, it will be reasonable to say that this sample contains mainly white phosphor.

Table 3.3 Mass ratios of white, red, blue, green and blue in fresh phosphor samples

Sample	1		2		3		4	
	g	wt%	g	wt%	g	wt%	g	wt%
White	0.425	80	0.35	60	0.275	40	0.1	20
Red	0.025	5	0.05	10	0.075	15	0.1	20
Green	0.025	5	0.05	10	0.075	15	0.1	20
Blue	0.025	5	0.05	10	0.075	15	0.1	20
Glass	0.025	5	0.05	10	0.075	15	0.1	20

To relate the amount of white phosphor and CaO content in the sample, four samples were prepared from different mass ratios of rare earth and impurities. Glass was also included in the sample in order to mimic the compositions in the used sample. The mixture formulas were shown in Table 3.3. All mixtures were elemental analyzed using the same procedures described above. Five calibration curves were plotted between rare elements in the mixture against rare earth or impurity contents in order to predict the mass ratio of either each phosphor or glass from the oxide of main element found in the bulk (see Figure 3.3 – 3.7). These calibration curves were found to be very useful and convenient to quantify mass ratio of main component (which could be either a kind of phosphor or glass) as well as minor components (which could be phosphors and/or glass). It was noticed that BaO was found only in blue phosphor. Thus it was suggested that blue phosphor might be one form of the derivatives of BaO.

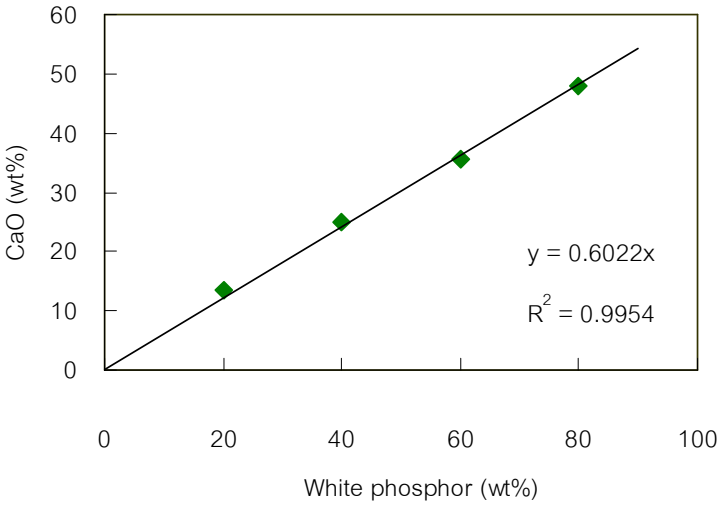

Figure 3.3 Relationship between mass ratios of CaO and white phosphor in the samples.

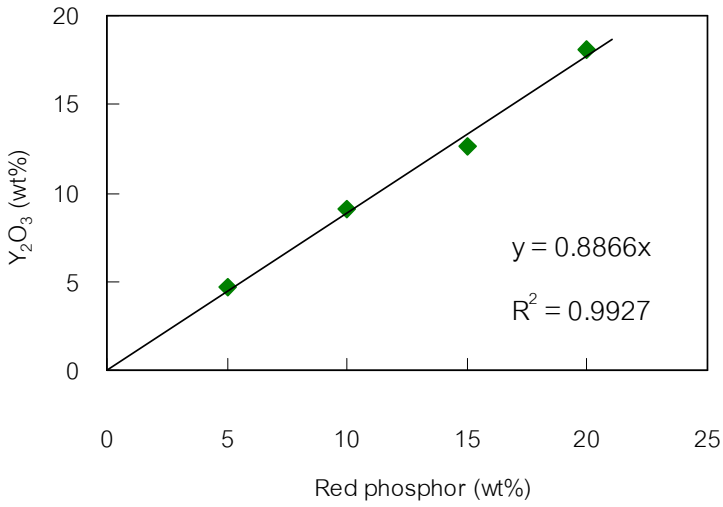

Figure 3.4 Relationship between mass ratios of Y_2O_3 and red phosphor in the samples.

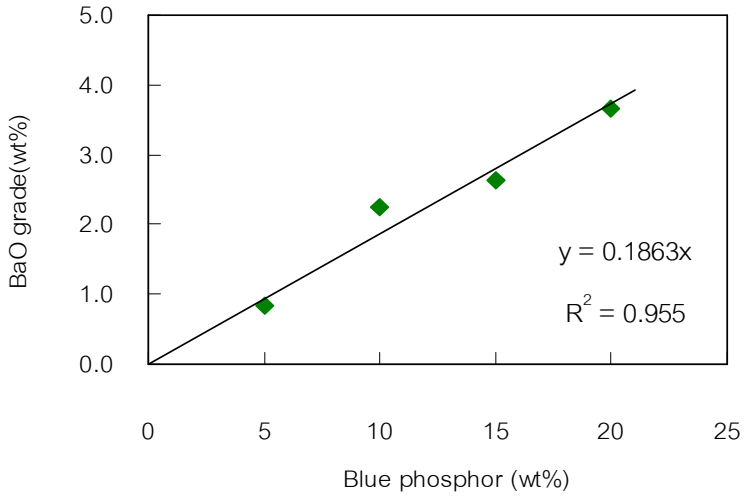

Figure 3.5 Relationship between mass ratios of BaO and blue phosphor in the samples.

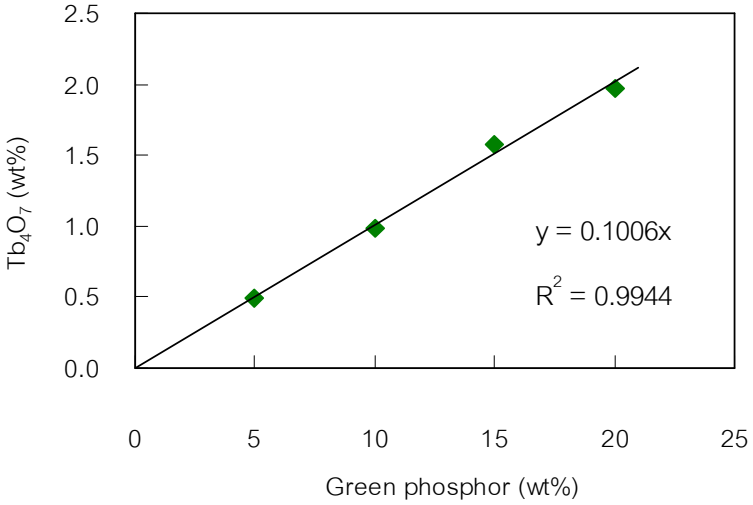

Figure 3.6 Relationship between mass ratios of Tb_4O_7 and green phosphor in the samples.

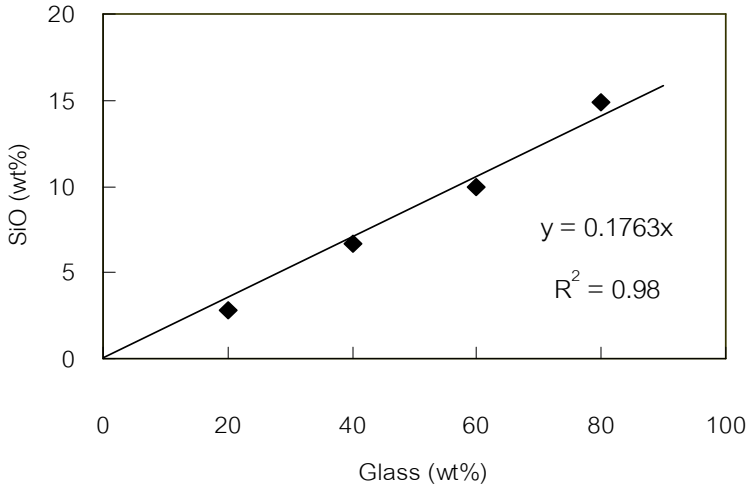

Figure 3.7 Relationship between mass ratios of SiO_2 and glass in the samples.

Linear relationship between mass ratio of phosphors and glass and their main elements were summarized below. All predicted equation was found to have relatively high correlation with the experimental data ($R^2 > 95\%$).

White Phosphor $y = 0.602x$; $R^2 = 0.995$ (3.1)

Red Phosphor $y = 0.886x$; $R^2 = 0.992$ (3.2)

Green Phosphor $y = 0.208x$; $R^2 = 0.985$ (3.3)

Blue Phosphor $y = 0.186x$; $R^2 = 0.955$ (3.4)

Glass $y = 0.176x$; $R^2 = 0.980$ (3.5)

Table 3.4 Elemental analysis of mercury-containing and mercury-free used phosphors

Mercury-containing used phosphor		Mercury-free used phosphor	
Element	Mass ratio (wt %)	Element	Mass ratio(wt %)
CaO	31.2	CaO	25.8
P_2O_5	26.1	P_2O_5	23.7
Y_2O_3	10.8	Y_2O_3	14.4
Al_2O_3	6.51	SiO_2	7.94
SiO_2	6.13	Al_2O_3	6.44
La_2O_3	4.27	La_2O_3	5.64
Na_2O	3.65	SrO	3.55
SrO	2.82	Na_2O	1.2
CeO_2	1.95	CeO_2	3.14
BaO	1.65	BaO	2.78
Tb_4O_7	1	Tb_4O_7	1.36
Eu_2O_3	0.915	Eu_2O_3	1.25
MgO	0.904	MgO	0.654
MnO	0.691	MnO	0.514
Sb_2O_3	0.408	Sb_2O_3	0.366
Others	1	Others	1.266

In this section, elemental analysis of the mercury-containing used phosphors and mercury-free one were conducted. Table 3.4 shows the compositions of both used samples. It was found that the results were quite similar even the mass ratios of some elements were slightly different. Since mecury has been recognized as a strong chemical hazard compound, using of mercury should be limited for safety purpose. Thus only mercury-free used phosphor was used as the representative for used phosphor samples in further experiments.

3.3.2 Particle size distribution

The range of particle size of interest in this experiment ranged between 5 to 20 μm. The size of rare earth phosphor particles were mostly (~80%) about 7 μm. Results show that the mass frequency of each particle size categorized as a function of particle size, commonly known as particles size distribution was most affected in shifting particle size distribution toward finer sizes. For example, Figure 3.8 shows a noticeable broader size distribution of white phosphor (4–20 μm) than the size distributions of blue (3-17 μm), red (2-13 μm) and green (2-9 μm) phosphors respectively. The median particle diameter (X_{50}), defined as the size in microns that splits the distribution with half above and half below this diameter, of each component was directly determined from the plot and found to be about 9.5, 8, 6 and 5 μm for white, blue, red and green phosphors respectively. Figure 3.9 shows particle size distribution frequency of all samples.

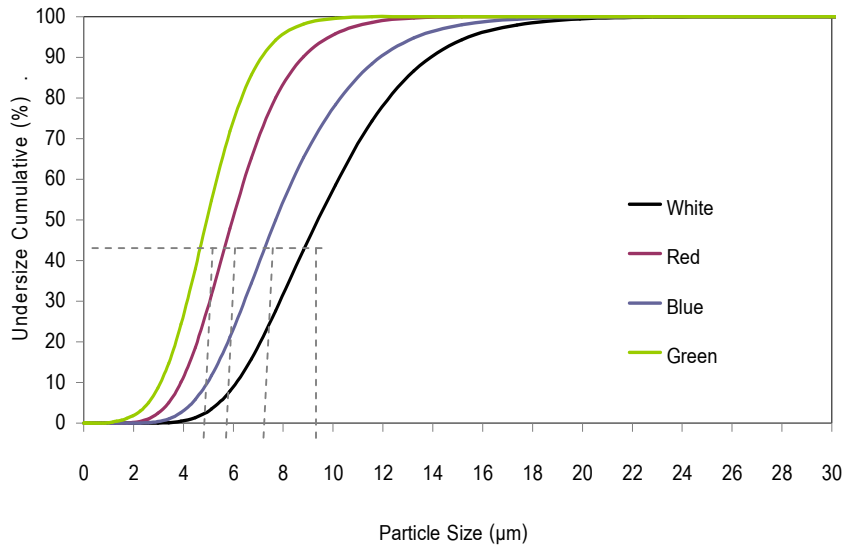

Figure 3.8 Undersize cumulative

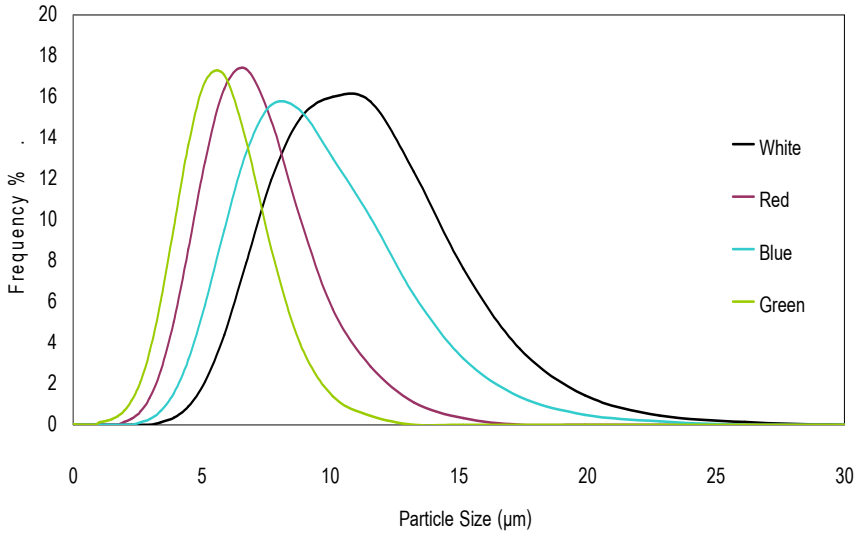

Figure 3.9 Particle size distributions

3.3.3 Specific gravity

Table 3.6 shows specific gravities of phosphors. Clearly, white phosphor had the lowest density of 3.28 g/cm^3 while red phosphor had the highest density of 5.34 g/cm^3. Since the densities of blue, red and green phosphors were significantly higher than the white one, it should be possible to separate impurity (which was white phosphor in this case) from the rare earth by a mean of gravitational technique.

Table 3.6 Specific gravity of phosphors

Sample	Specific Gravity (g/cm^3)
White Phosphor	3.28
Red phosphor	5.34
Blue phosphor	5.33
Green phosphor	3.91

3.3.4 Morphology investigation

To further characterize the sample, SEM images of all species were taken. Figure 3.10 shows structure of each sample. White phosphor has the biggest size of over 5 μm while red, blue and green phosphors had similar size (about 2-5 μm). It was observed from the images that when the particle size became smaller, more self-aggregations were formed. Thus the processor should carefully design the sifting separation process.

Figure 3.11 shows images from mercury-free used sample with different magnifications of x500, x1000, x2000 and x4000. It was observed from Figure 3.12 that

the apparent size of self-aggregated phosphor particles size and CaO were almost similar. Therefore, particle dispersion will become important factor to improve separation efficiency. Other blue, red, green phosphors particles are much smaller than white phosphor (CaO).

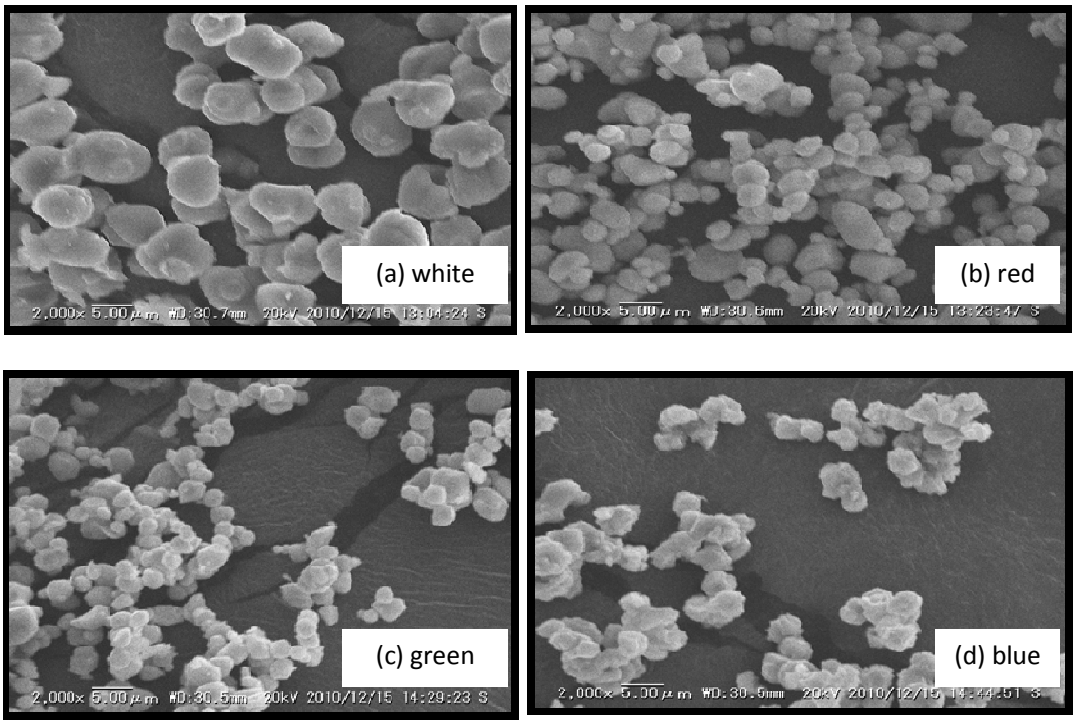

Figure 3.10 SEM images of fresh samples (a, b, c and d having the same magnification 2000x5.00μm)

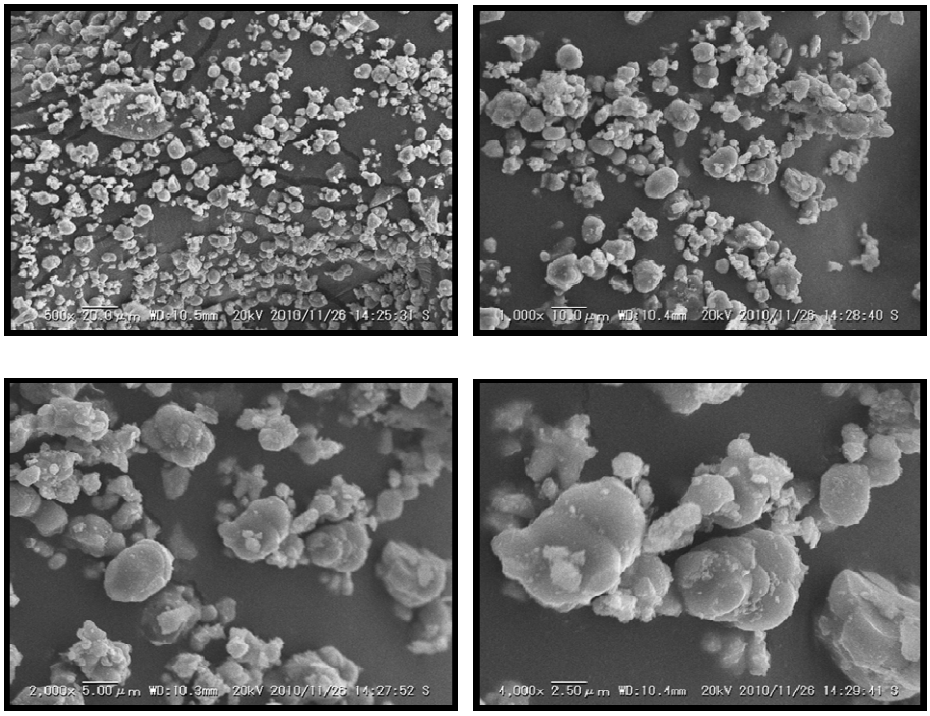

Figure 3.11 SEM images of used samples with different magnifications

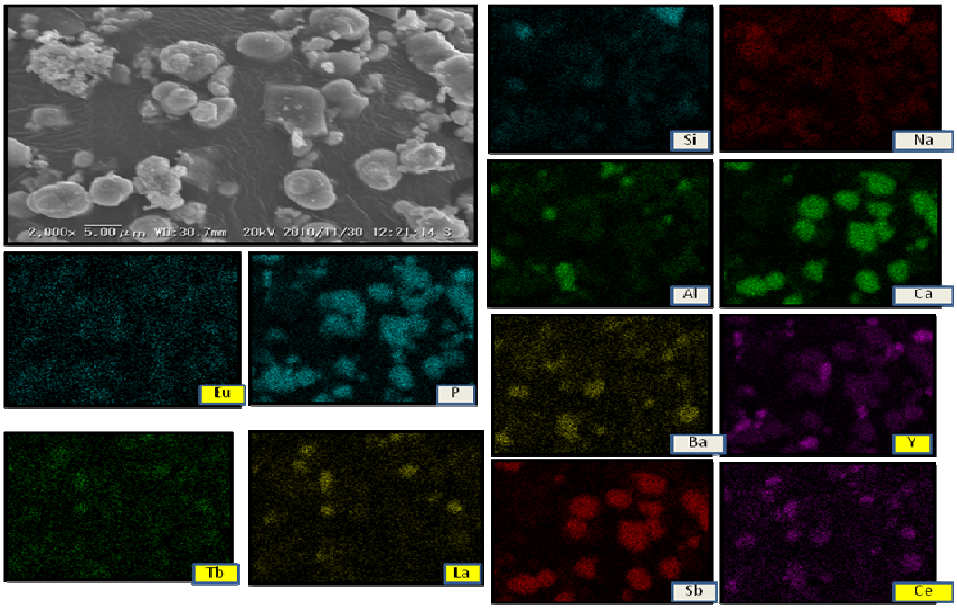

Figure 3.12 SEM-EDX images of used sample and its contained elements

3.4 Conclusions

X-ray fluorescent spectrometer (XRF) analysis showed the analysis of REE in fresh and used samples. From XRF analysis, white phosphor was found to be a main component of fluorescent lamp but did not contain rare earth element. In contrast, red phosphor contained 92.17% Y_2O_3 and 7.59% Eu_2O_3; blue phosphor contained 0.0272% Y_2O_3 and 5.45% Eu_2O_3; and green phosphor contained 42.9% La_2O_3, 19.8% CeO_2 and 10.7% Tb_4O_7. Calibration curves with >95% correlation co efficiency that related the quantity of main elements in the bulk with the amount of interested phosphors and glass were also developed. All calibration curves exhibited strong linear relationships between mass fraction of element and mass of phosphors or glass in the bulk.

When used phosphors were tested for their compositions, results also revealed that mercury-free used phosphors contained rare earth elements, 14.4 wt% Y_2O_3, 3.14wt% CeO_2, 1.36 wt% Tb_4O_7, 1.25 wt% Eu_2O_3 and 5.64 wt% La_2O_3. This confirmed that used phosphor from industrial waste could be considered as an abundant source for rare earth elements. However, since the main element found in white phosphor was CaO, white phosphor particles were thus fragile and could be easily broken when they were subjected to mechanical stress. This suggestion was confirmed by SEM-EDX images. The broken particles could favored clogging during sieving operation and thus could be a serious problem that should be prevented.

Particle size distribution and specific gravity of fresh phosphor analysis showed that white phosphor particles were larger than the others, while its specific gravity was the lowest one. All results suggested that there were significantly differences in physical properties, e.g. particle size and specific gravity, between white phosphor particles and others. Thus it should be possible that sieving and air classifier could be alternative methods that can be employed to separate the rare earth elements form white phosphor

and glass. In the next sections the separation process were tested to verify this assumption.

CHAPTER IV

SEPARATION OF RARE EARTH OXIDES

In previous chapter, elemental analysis of used phosphors confirmed that the recycled materials contained impurities (white phosphor and glass), mixed with enrichment of rare earth elements. Fortunately, the results also confirmed that rare earth elements (red, blue and green phosphors) are smaller than impurities (white phosphor and glass). Moreover, white phosphor had much lower specific gravity than rare earth elements. This hinted us that suitable physical separation methods might be applied to purify the rare earth elements.

Sieving and screening are unit operations that can be used to physically separate interested particles from the bulk. They are traditional methods that are most widely used to separate solid particles in the bulk by size exclusion technique. Sieving is generally used to refer to a batch process while the term screening is usually used when the sizing operation is continuous (Liu et al., 2009). Because of their simplicities, sieving and screening are commonly used, both industrially and academically, for the classification of particulate materials.

Basic sieving/screening configuration generally consists of a series of different sieve openings that are stacked layer by layer, from the largest opening holes at the top to the finest opening holes at the bottom. Sample to be separated is fed on the top sieve opening. The stack is tamped or vibrated to facilitate the movement of the powder downward. The particles are consequently separated by their sizes, from bigger to smaller particles. The residual left on each sieve can be quantified in order to extract particle size distribution in the bulk sample.

In this chapter, dry, wet and air sieving techniques were employed to verify this assumption. Optimum sieving conditions of were investigated. Only used phosphor was tested through out this section as the main target of this study was to recover rare earth elements from this kind of industrial waste.

4.1 Dry Sieving

For dry sieving, machines that are generally employed are vibrating and ultrasonic sieving machines. The former is a basic sieving device that performs sieving by horizontally moving or shaking the sieve set at the pre-set vibration amplitude and time. The latter, ultrasonic sieving machine is a more advance machine that takes an advantage of using sound wave at a range of specific frequency together with vertical movement of the sieve set to perform sieving. In this subsection the optimum conditions of both methods were addressed.

4.1.1 Vibration sieving

4.1.1.1 Instrument

1. Vibration Sieving Machine (Fritsch DK004AM, Germany)

Figure 4.1 Vibration sieving machine and sieve opening 20, 16, 12.5, 10, 8 and 5 μm

2. Sieve opening 20, 16, 12.5, 10, 8 and 5 μm (Tsutsui, Japan)

3. X-ray fluorescent spectrometer

4.1.1.2 Experiment

The basic configuration of vibration sieving was shown in Figure 4.2. From top to bottom, the order of sieve opening was 20, 16, 12.5, 10, 8 and 5 μm, respectively. 20 g of mercury-free used phosphors was fed and separated at a vibration amplitude of 1.0, 2.0 and 3.0 mm. Time of sieving was kept constant at 60 min.

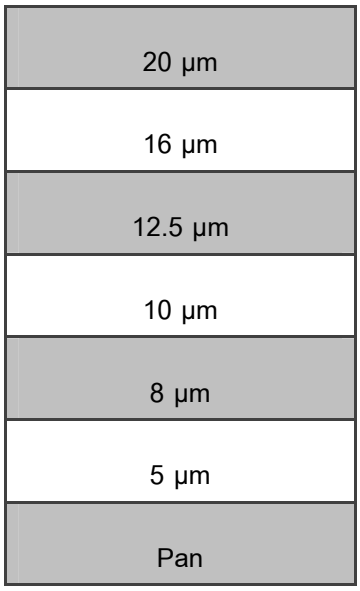

Figure 4.2 Basic set up of vibration sieving openings

After sieving, the yield, defined as the mass fraction of the residuals on each sieve, was calculated as the ratio between the mass of the residual to the total mass of the bulk (20g) as shown in equation 4.1:

$$\text{Yield} = \frac{x}{20} \times 100\% \tag{4.1}$$

where x is the mass of the residual (g). The residuals on each sieve were then pulverized in a mortar and elemental analyzed using XRF. The calibration curves developed in Chapter II were then used to estimate the mass fraction of each phosphor and/or glass in the residuals.

4.1.1.3 Results and discussion

- **Yield**

Table 4.1 shows residual's mass and yield, categorized by particle size (or sieve opening size). Figure 4.3 was plotted from information in Table 4.1 for a better visualization of the size-distribution trends at all vibration amplitudes. As shown in Figure 4.3, all results were quite similar. It seemed that vibration slightly affected the yield as indicated by a decrease in the yield of particles that were larger than 20 μm with an increase in vibration amplitude. The yield of 30% at the lowest vibration amplitude was reduced to 25% at the vibration amplitude of 2 mm and further slightly reduced to 24% at the maximum vibration amplitude.

Table 4.1 Residual's mass and yield at different vibration amplitude

Particle size (μm)	Vibration amplitude (mm)					
	1		2		3	
	Mass (g)	Yield (wt%)	Mass (g)	Yield (wt%)	Mass (g)	Yield (wt%)
+20	6.30	31.17	5.34	25.39	4.80	24.13
-20+16	10.55	52.20	12.82	60.96	11.36	57.11
-16+12.5	3.22	15.93	1.69	8.04	3.68	18.50
-12.5+10	0.05	0.25	0.98	4.66	0.05	0.25
-10+8	0.05	0.25	0.00	0.00	0.00	0.00
-8+5	0.04	0.20	0.00	0.00	0.00	0.00
-5	0.00	0.00	0.20	0.95	0.00	0.00

However, in all cases, less than 1% of samples could pass through the 10-μm sieve opening. This result agreed well with the information extracted from SEM images in Chapter IV (Figure 4.9). Even most of (single) particles are smaller than 10 μm, the self-aggregation of particles resulted in bigger particles formation which could not pass through the target sieve opening. Even maximum vibration magnitude applied to the operation in this experiment was seemed to be insufficient to disperse these aggregated particles.

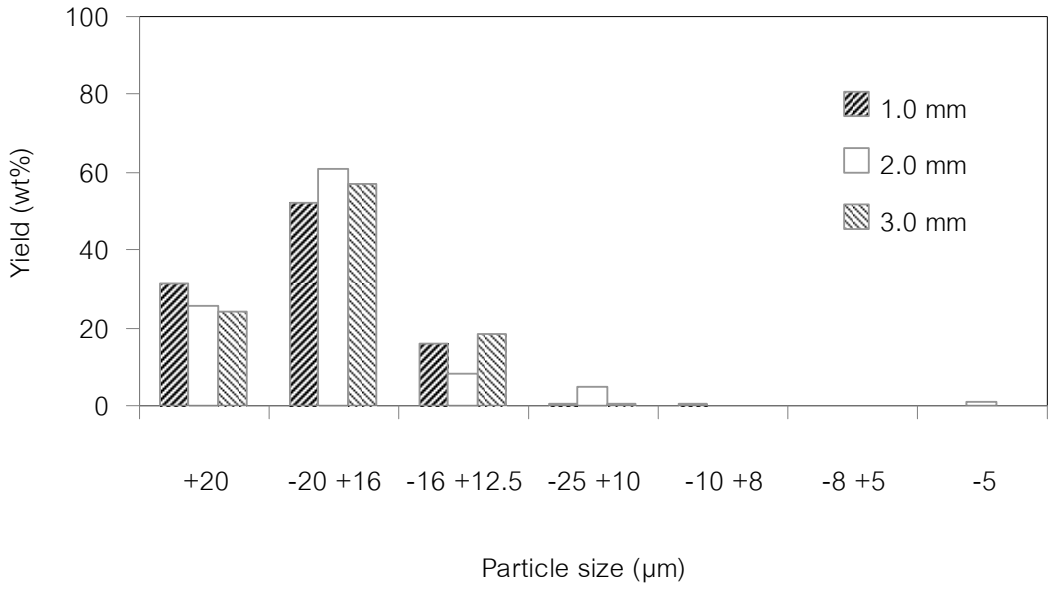

Figure 4.3 Yields obtained at different vibration amplitudes

- **Elemental Analysis**

After sieving, the quantity of white, red, blue, green phosphors and glass in residual on each sieve opening were determined using equations 2.1, 2.2, 2.3, 2.4 and 2.5. Figure 4.4 shows approximate mass fraction of rare earth elements in the yields obtained from vibration sieving under different vibration amplitudes. It was found that were the mass fraction of rare earth element was about 20% of the total mass of the yields, regardless of vibration amplitudes or sieve opening sizes.

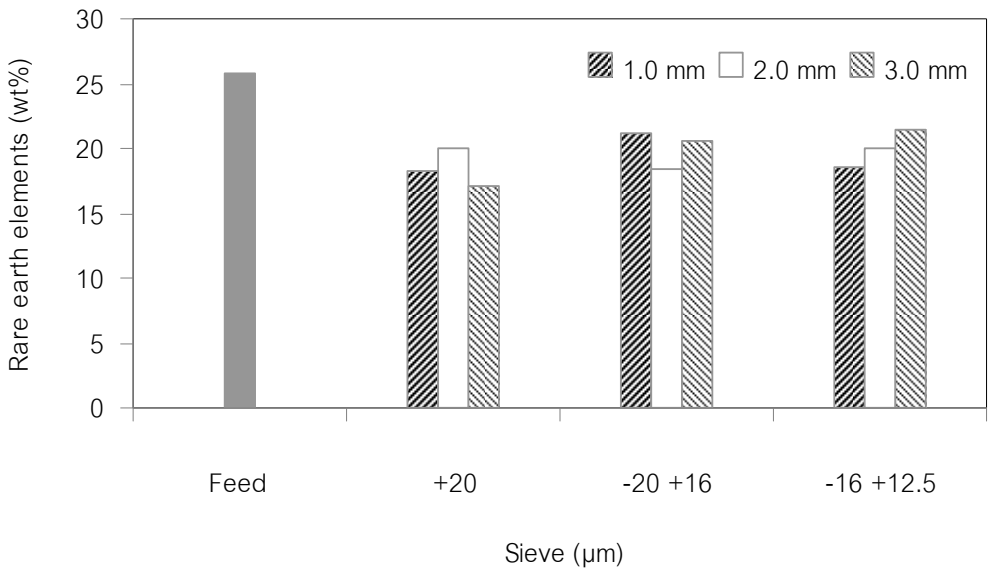

Figure 4.4 Effects of vibration amplitude on the quantity of rare earth elements

However, there was a slight difference in the mass fraction of white phosphor in the yields obtained from different sieve openings. For the yield from the 20-μm sieve, mass fraction of white phosphor was about 50% (Figure 4.5). The mass fractions of white phosphor were then increased to about 60% in the yields obtained from the 16-μm and 12.5-μm sieves, no matter what the vibration amplitude was. The main element found in white phosphor was CaO which was fragile. During sieving white phosphor particles could be broken into small pieces and pass through the sieve opening. This could be a reason that white phosphor's mass fraction on the yields obtained from smaller sieve openings was slightly higher than the one obtained from larger sieve opening. This evidence led to a conclusion that vibration sieving under sieving conditions used in this experiment was not a suitable method to separate white phosphor from the targeted rare earth elements.

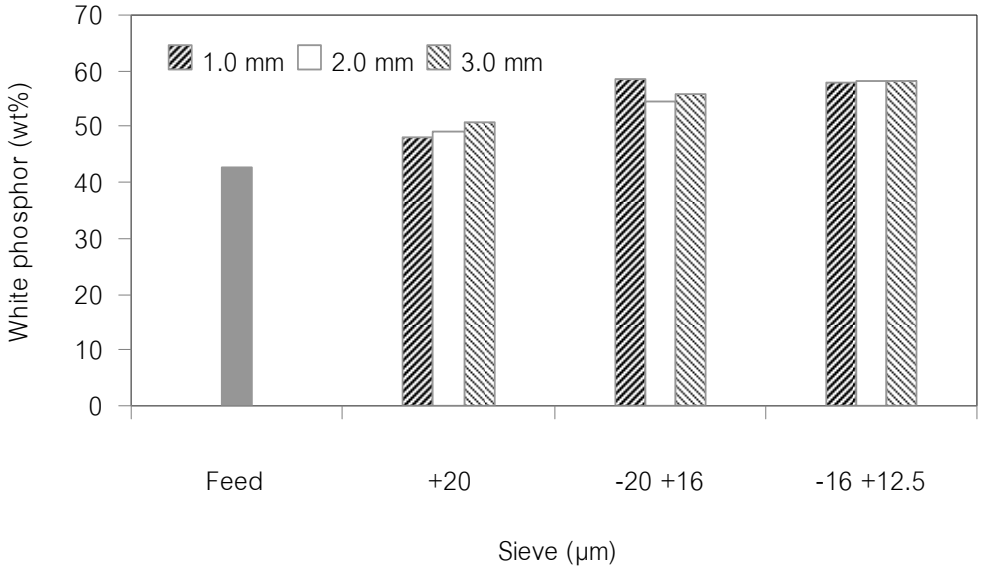

Figure 4.5 Effects of vibration amplitude on the quantity of white phosphor

Figure 4.6 shows SiO_2 content in the yields. Differently from white phosphor, silica oxide was effectively separated using a 20-μm sieve opening and consequently a 16-μm sieve opening. The mass fraction of silica oxide decreased from 13 wt% on a 20-μm sieve opening to about 4 wt% on 16-μm sieve opening and finally less than 3 wt% on 12.5-μm sieve opening.

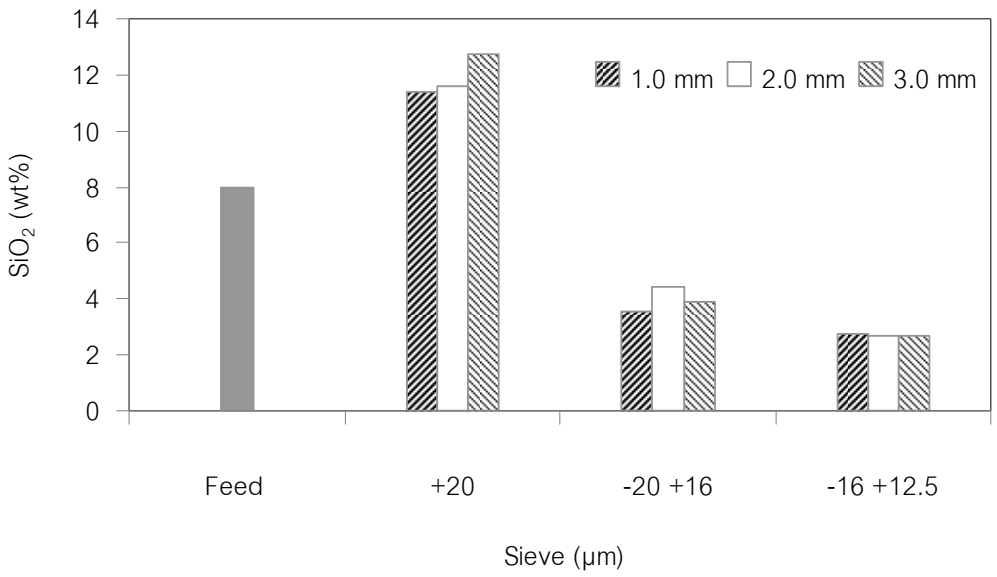

Figure 4.6 Effects of vibration amplitude on the quantity of SiO_2 grade

However, the horizontal movement generally has a disadvantage. Since particles are forced to move across sieve's surface, some particles particularly those having size closed to mesh size tend to block sieve's apertures, leading to sieve blinding or clogging. Tapping action apparently reinforces the vertical movement, and at the same time helps in dislodging particles that blocked apertures, and thus reduces the sieve blinding effect. This explains why tapping has a profound effect on sieving efficiency as compared with the no-tapping option (Liu et al., 2009). However, at this step our objective which was to separate the rare earth elements from the used samples had not been fulfilled yet. This was because white phosphors still contaminated in all size of yields at relatively high percentage. Other effective methods were still needed to be investigated and were discussed in next subsections.

4.1.2 Ultrasonic Several Sieving

4.1.2.1 Instrument

1. Ultrasonic Sieving Machine (Tsutsui 20AT, Japan)

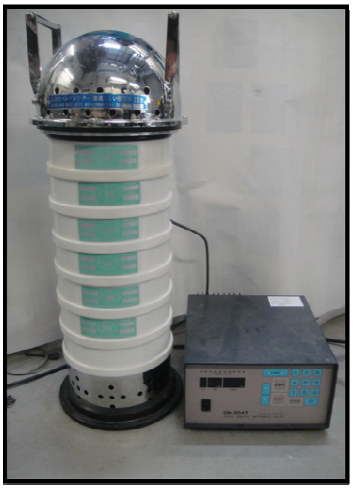

Figure 4.7 Ultrasonic sieving

2. Sieve opening 20, 16, 12.5, 10, 8 and 5 μm (Tsutsui, Japan)

3. X-ray fluorescent spectrometer

4. Ceramic Balls

4.1.2.2 Experiment

Basic configuration of ultrasonic sieving was similar to vibration sieving set up shown in Figure 4.2 (Figure 4.7). During sieving, sound wave was also applied to the samples. Along the process, sound wave frequency was not constant but was gradually

increased every 3 min, from 50 to 100, 120, 150 and 170 Hz. Three levels of sieving time were investigated: 5 (1x5), 10 (2x5) and 15 min (3x5).

In order to prevent clogging during sieving, a number of ceramic balls (diameter of 2-3 mm) were additionally mixed with samples in order to disperse particle agglomeration (especially for small particles as mentioned in the last chapter) (see Figure 4.8). The usage of ceramic balls was about 20 g per 20 g of sample's mass (1:1). For comparison purpose, same experiment was also conducted but without the using of ceramic balls.

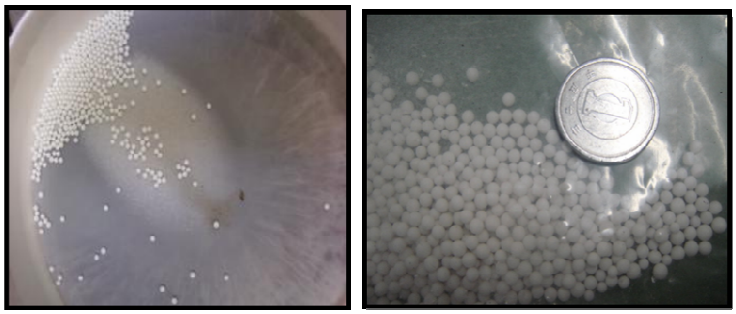

Figure 4.8 Appearance of ceramic balls

Quantification of phosphors and glass in the residuals on each sieve were then examined using the same procedures described in vibration sieving section.

4.1.2.3 Results and Discussion

- Yield

In the first part of ultrasonic sieving experiment, effect of dispersive agent (the ceramic balls) on yield's quantity was studied. Table 4.2 shows mass fraction of residuals on each sieve opening and Figure 4.9 shows the effect of ceramic balls on

particle size distribution. Clearly, smaller sizes of yields increased when ceramic balls were used. This indicated that ceramic balls effectively decreased particle aggregations. Without the balls, it was impossible that particles could pass through sieve opening with a hole-size of 10 μm or smaller. Using ceramic balls boosted separation efficiency as reflected from the yield of about 50% for particle smaller than 10 μm. So, it was suggested here that using of ultrasonic sieving with ceramic balls as a dispersive agent would separation efficiency and improved yield. Thus, ultrasonic sieving with ceramic balls was selected as a standard process.

Table 4.2 shows sample weight and yield of with balls and without balls.

Particle size (μm)	With ball		Without balls	
	Mass (g)	Yield (wt%)	Mass (g)	Yield (wt%)
+20	1.12	5.63	5.57	27.88
-20 +16	0.75	3.77	8.28	41.44
-16 +12.5	2.84	14.27	5.45	27.28
-12.5 +10	5.24	26.33	0.68	3.40
-10 +8	3.28	16.48	0	0.00
-8 +5	3.46	17.39	0	0.00
-5	3.21	16.13	0	0.00

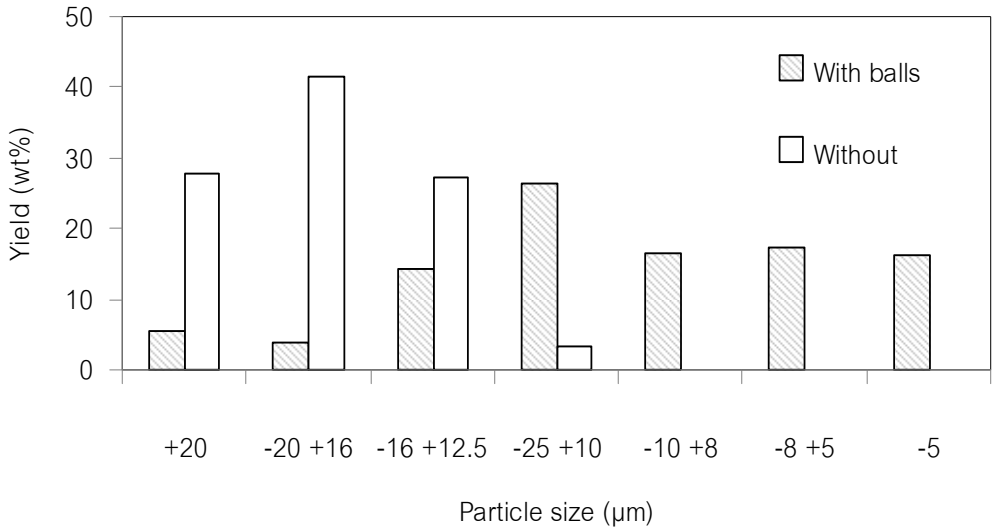

Figure 4.9 Dependencies of particle size distribution on dispersive agents (ceramic balls)

Table 4.3 and Figure 4.10 show the effects of sieving time on mass fraction and yield of various particle sizes. When total operating time was 5 minutes, the percentage of particles that were larger than 10 μm was higher that 70%. This implied that sieving time was probably insufficient. On the other hand, when sieving time was increased to 10 or 15 min, the percentage of those large particles was reduced to less than 50%.

Table 4.3 Residual's mass and yield of the sample at different sieving time.

Particle size (μm)	Sieving time: 1x5 min		Sieving time: 2x5 min		Sieving time: 3x5 min	
	Mass (g)	Yield (wt%)	Mass (g)	Yield (wt%)	Mass (g)	Yield (wt%)
+20	1.26	6.24	1.2	5.96	1.12	5.63
-20 +16	1.71	8.47	0.62	3.08	0.75	3.77
-16 +12.5	3.75	18.56	1.13	5.61	2.84	14.27
-12.5 +10	8.16	40.40	5.2	25.81	5.24	26.33
-10 +8	2.5	12.38	4.43	21.99	3.28	16.48
-8 +5	1.62	8.02	4.05	20.10	3.46	17.39
-5	1.2	5.94	3.52	17.47	3.21	16.13

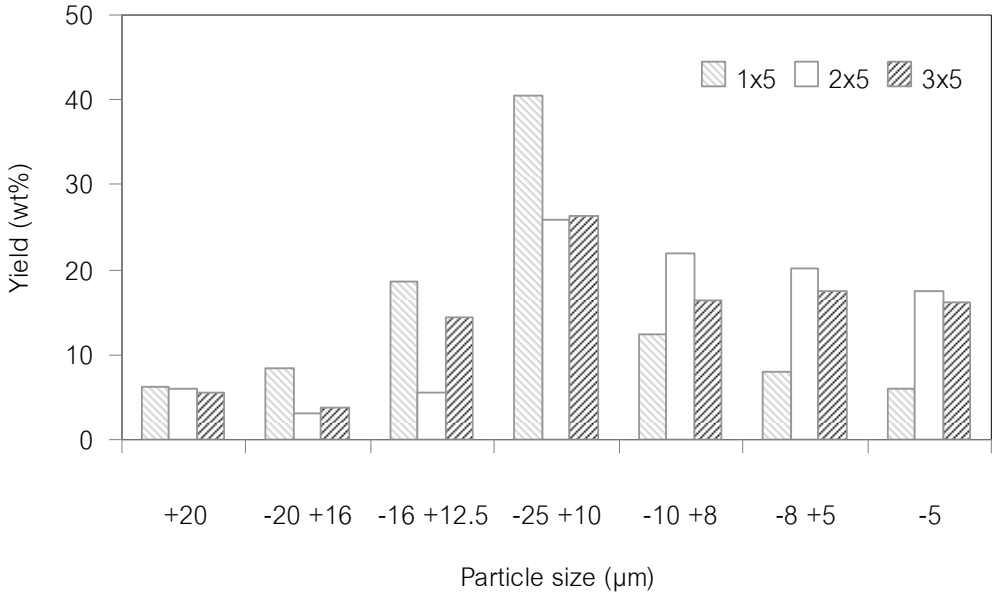

Figure 4.10 Effect of sieving time on particle size exclusion

- Elemental Analysis

In this subsection, the capability of ultrasonic sieving and effect of dispersive agent (ceramic balls) on separation performances were investigated. Figure 4.11 shows the effects of dispersive agent on the rare-earth-element contents in the yields. Without using ceramic balls in ultrasonic sieving, mass fraction of rare earth elements was quite similar to vibration sieving. However, when ceramic balls were mixed together with the used sample to be ultrasonically sieved, the mass fraction of rare earth elements was noticeably higher. As categorized by yield's size, the rare-earth-element content was 22.72 wt% and 23.41 wt% in "+5 -8 μm" yield and "-5 μm" yield, respectively. In another word, rare earth elements in the interval sieve below 8 μm were more than 40 wt%. This shows that ultrasonic sieving with dispersive agent could enrich rare-earth-element contents in the yields.

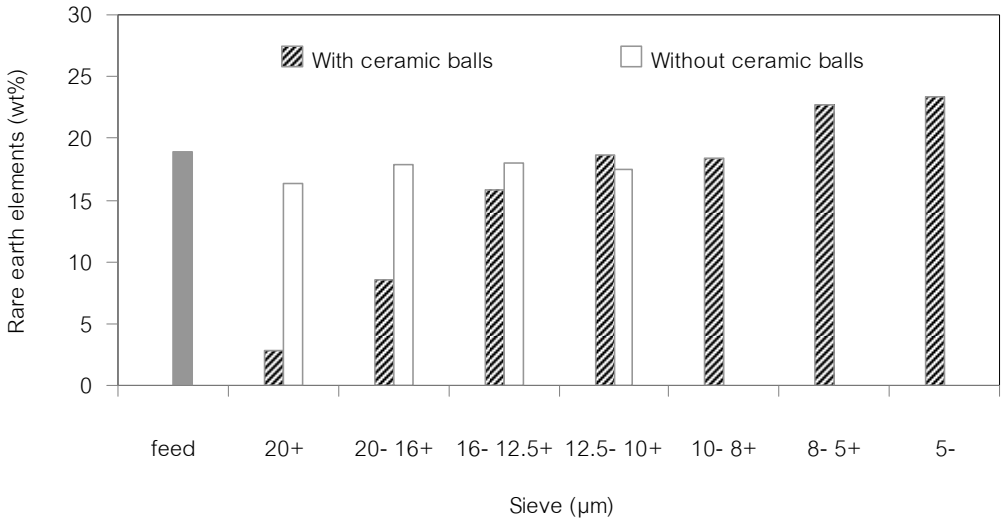

Figure 4.11 Effects of dispersive agent on the rare-earth-element contents in the yields.

Figure 4.12 shows the effects of dispersive agent on white phosphor contents in the yields. The mass fractions of white phosphor in the yields obtained after ultrasonic sieving without balls were similar to those obtained after vibration sieving.

While ultrasonic sieving with ceramic balls enriched rare-earth-element contents, it showed an adverse effect on white phosphor separation. Ultrasonic vibration sieving with balls resulted in white phosphor content approximately 50 wt% in the yield's size below 12.5 μm. Moreover, white phosphor was found to be abundant even in sieving section 5 μm. This could be due to an effect of ceramic balls that crushed enriched-CaO white phosphor particles and dispersed agglomeration particles. This could be the problem since broken white phosphor particles could mix with rare earth elements even in the finest stage.

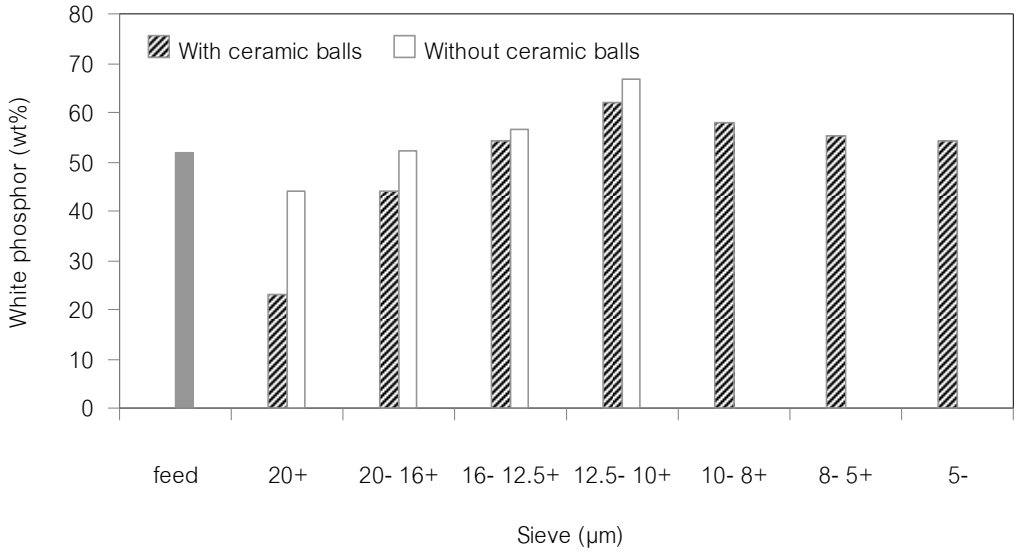

Figure 4.12 Effects of dispersive agent on white-phosphor contents in the yields.

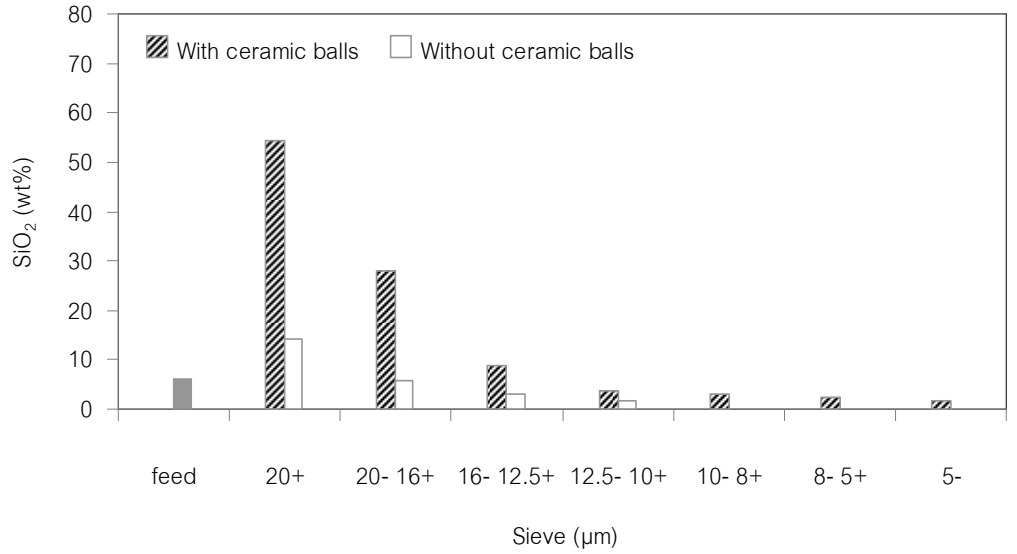

Figure 4.13 Effects of dispersive agent on SiO_2 contents in the yields

To investigate effects of dispersive agent on silica oxide contents in the yields, Figure 4.13 was plotted. With ceramic balls, much higher quantity of SiO_2 was obtained from the yields on +20 μm size sieve compare to SiO_2 content obtained from yields collected after ultrasonic sieving without balls. In s range of -20 +16 μm quantity of SiO_2 is approximately 28 wt%. Therefore ultrasonic vibration with balls was probably an effective method to reduce impurities of glass in the used samples.

Finally, effect of sieving time on the rare earth separation was investigated. From Chapter III, characterization of fresh sample mentioned that the size of rare-earth-element particles was almost below 7 μm. Figure 4.14 shows effects of sieving time on the rare-earth-element contents in the yields. From all sieves having size below 8 μm, rare earth element content was over 20 wt%. In overall, sieving time had no significant effect on rear earth separation from the fact that rear-earth-element mass fraction in the yields after sieving for 1, 2 and 3 times are not quite different, regardless the yield's size or sieving time were.

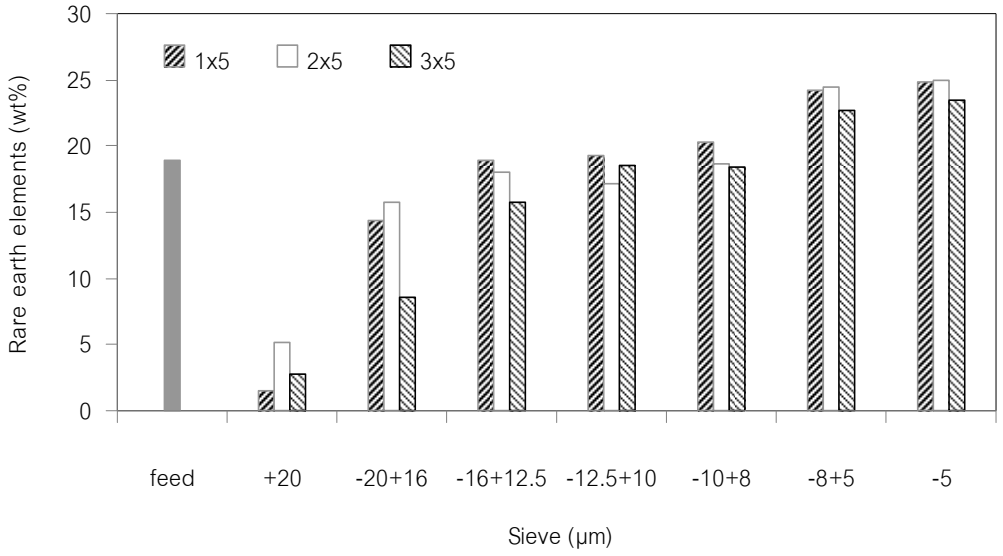

Figure 4.14 Effects of sieving time on the rare-earth-element contents in the yields.

Figure 4.15 shows that sieving time nearly did not affect the mass fraction of white phosphor in the yields. Similar result was found in a case of mass fraction of SiO_2 as well (see Figure 4.16).

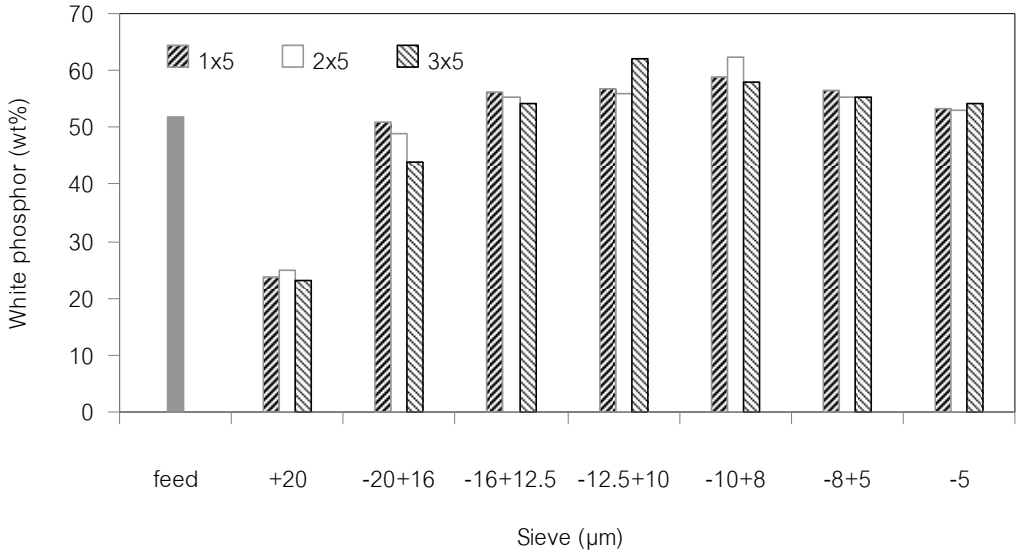

Figure 4.15 Effects of sieving time on white-phosphor grade contents in the yields

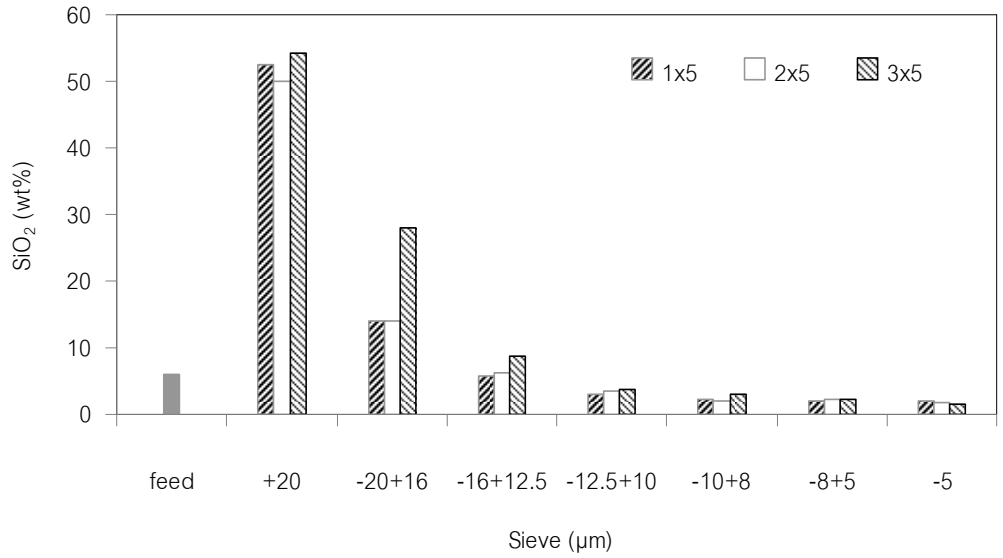

Figure 4.16 Effects of sieving time on SiO_2 contents in the yields

4.1.3 Ultrasonic single sieving

Before continuing the experiment section, it was worthy to mention about the theoretical background related to the separation capability of sieving processes. The term “Newton’s efficiency” is well-recognized as a parameter that indicates the effectiveness of a separation process and is formulated according to equation 4.2 (Petrus et al., 2010):

$$\eta_N = R_r - (1 - R_{nr}) \tag{4.2}$$

where η_N is Newton's efficiency, R_r is the recovery rate of rare earth element in the undersized product (%) and R_{nr} is the recovery of non-rare earth element in the oversized product (%).

The recovery of rare earth element may be further formulated in term of material balance, based on the rare earth element in the feed, oversize and undersize products as expressed by equation 4.3 and 4.4

$$R_r = \frac{C_r W_r}{C_f W_f} = \frac{(C_f - C_{nr})C_r}{(C_r - C_{nr})C_f} \times 100\% \tag{4.3}$$

$$R_{nr} = \frac{W_{nr}(1 - C_{nr})}{W_f(1 - C_f)} = \frac{(C_f - C_r)(1 - C_{nr})}{(C_{nr} - C_r)(1 - C_f)} \times 100\% \tag{4.4}$$

where W_f is the mass of feed (kg), W_r is the mass of rare earth element product (undersize or oversize) (kg), W_{nr} is the mass of non rare earth element product (undersize or oversize) (kg), C_f is the concentration of rare earth element in feed (%), C_r is the concentration of rare earth element in rare earth element concentrated product (%) and C_{nr} is the concentration of rare earth element in non rare earth element product (%).

Now let’s move to the experimental part. In previous subsections, vibration and ultrasonic sieving were tested in many conditions. Unfortunately, it was found that

vibration sieving cannot improve recovery percentage of rare earth elements while ultrasonic sieving alone without dispersive balls did not provide better results than vibration sieving. Even ultrasonic sieving with dispersive ceramic balls helped disperse the agglomerated particles and increase yield weight on small sieve openings, white phosphor was noticeably broken during sieving thus contaminated in the products. Only glass could be effectively separated even using relatively large sieve opening.

In this subsection, ultrasonic single sieving was employed in order to minimize mechanical damages of white phosphor and to improve rare earth purity. We focused on small sieve openings between 5 -12.5 μm with the expectation that impurities (glass and white phosphor) would be separated more effectively.

4.1.3.1 Instrument

1. Ultrasonic Sieving Machine (Tsutsui 20AT, Japan)

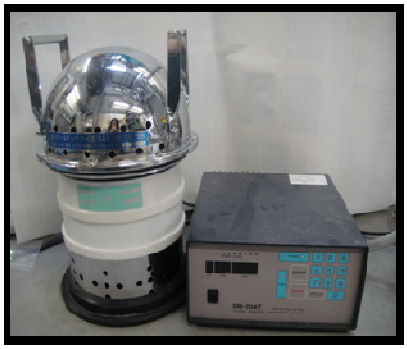

Figure 4.17 Ultrasonic single sieving

2. Sieve opening 20, 16, 12.5, 10, 8 and 5 μm (Tsutsui, Japan)

3. X-ray fluorescent spectrometer

4. Ceramic Balls

4.1.3.2 Experiment

The condition set for ultrasonic single sieving experiment was the same as the optimum condition obtained from ultrasonic (multi-)sieving experiment in subsection 4.1.2. Sieving time was set to be 10 (2x5) min. As mentioned, sound wave frequency was gradually increased every 3 min, from 50 to 100, 120, 150 and 170 Hz. Ceramic balls was mixed with mercury-free used phosphor sample at the same mass ratio (20 g : 20 g).

After sieving apparatus, the obtained yield remained on each sieve (12.5, 10, 8 and 5 μm) was pulverized in a mortar for 30 minutes for an elemental analysis using an X-ray fluorescence spectrometer (XRF). Thereafter, quantity of each phosphor was estimated using predicted equations 2.1, 2.2, 2.3, 2.4 and 2.5 obtained from the calibration curves developed in Chapter II and the concentration of rare earth elements was evaluated.

4.1.3.3 Results and Discussion

- Yield

Table 4.1 shows mass and yield the residual on each sieve while the oversized and undersized yields were summarized in Figure 4.18 for a better visualization. As expected, maximum and minimum oversized yields were obtained on 5-μm and 12- μm, respectively.

Table 4.4 Mass and yields on each sieve

Sieve Size (μm)	5 μm		8 μm		10 μm		12.5 μm	
	Mass (g)	Yield (wt%)	Mass (g)	Yield (wt%)	Mass (g)	Yield (wt%)	Mass (g)	Yield (wt%)
Oversize	11.88	67.73	10.04	56.03	4.84	25.85	3.17	15.94
Undersize	5.66	32.27	7.88	43.97	13.88	74.15	16.72	84.06

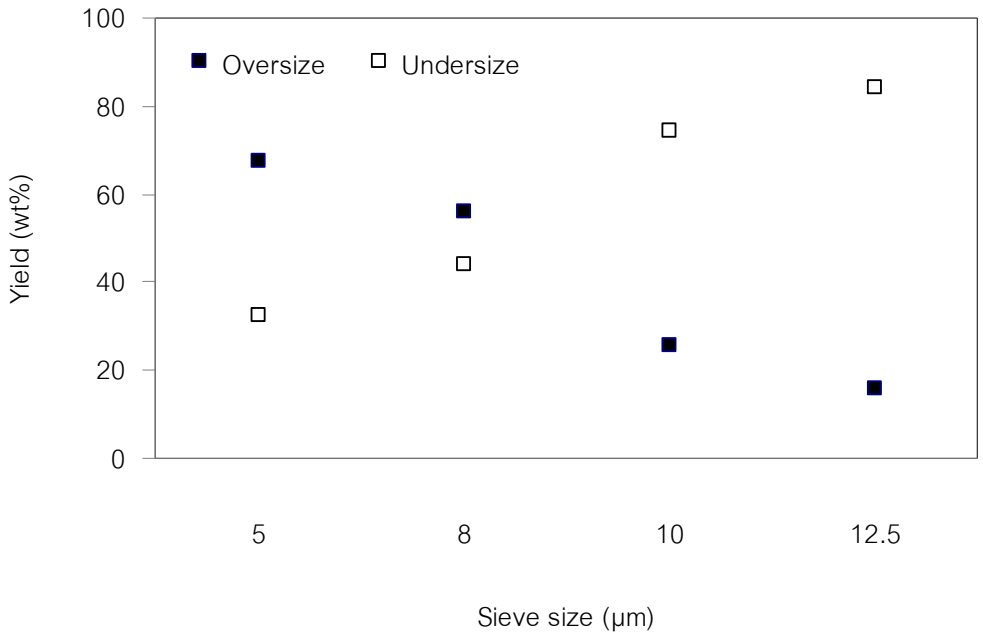

Figure 4.18 Yields obtained from each sieve from ultrasonic sieving

- Elemental Analysis

Yield of rare earth element were presented in Figure 4.19. The larger the sieve opening size was, the lower the oversized yield. Mass fraction of rear earth element in oversized and undersized yields was shown in Figure 4.19. In all cases the percentages of rear earth element in undersized yields were higher than the percentages of rear earth element in oversized yields. The highest mass fraction of rear earth element in yields of 33 wt% was achieved when the smallest sieve aperture (5 μm) was used.

Figure 4.20 shows the recovery rate of rear earth element from undersized yield. More than 95 wt% of rear earth element was recovered from the yield having size smaller than 12 μm. When slightly smaller sieve aperture of 10 μm was used, the recover rate decreased to about 85 wt%. The recovery rate decreased to 42 wt% when the smallest sieve aperture was used.

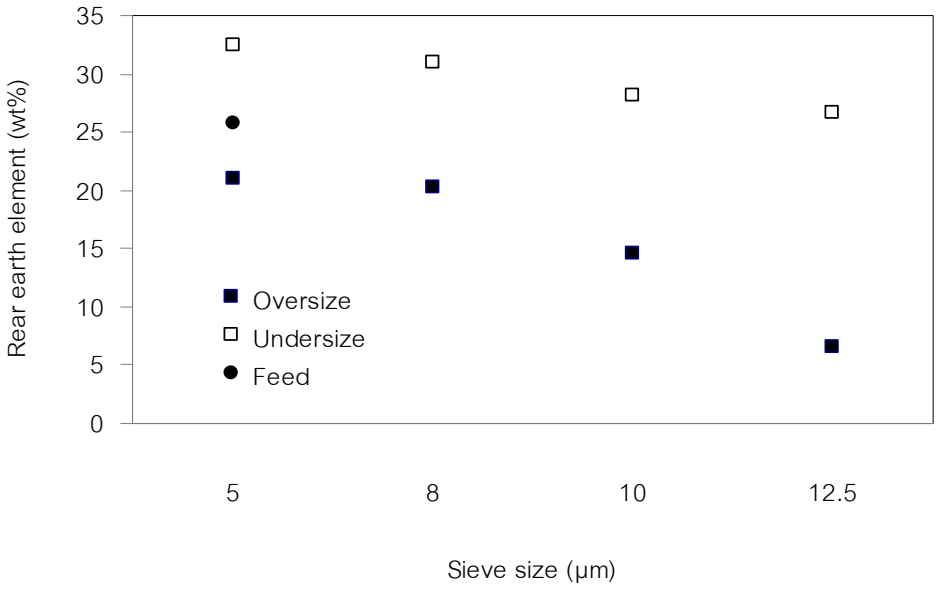

Figure 4.19 Oversized and undersized rare earth elements

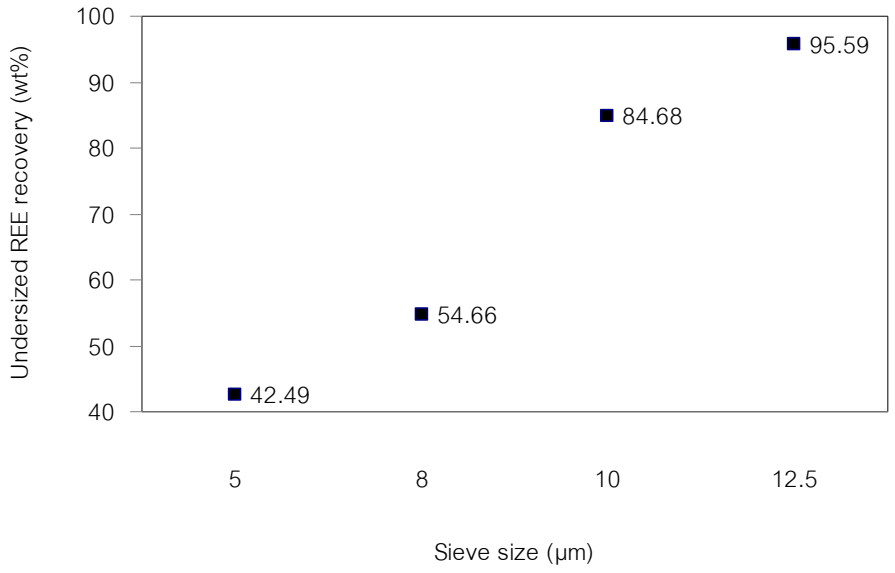

Figure 4.20 Recovery rate of undersized rare earth element

White-phosphor impurity was estimated from CaO content using the aforementioned method. Recovery rate of white phosphor was shown in Figure 4.21 and Figure 4.22. For sieve opening from 10 μm, the mass fractions of white phosphor in the oversized yields were lower than those in undersized yields, the fact that indicated an insufficient capability of the separation process. On the other hand, the mass fractions of white phosphor in oversized yields obtained from 5-μm and 8-μm became slightly higher than the mass fractions of white phosphor in undersized yields. This reflected to the improvements of white phosphor separation capability when smaller sieve sizes were used. Even the mass fractions of white phosphor from 8-μm and 5-μm sieves were not quite different; the recovery rate of white phosphor from the yields obtained from a 5-μm sieve was noticeably higher than the sample obtained from 8-μm sieve.

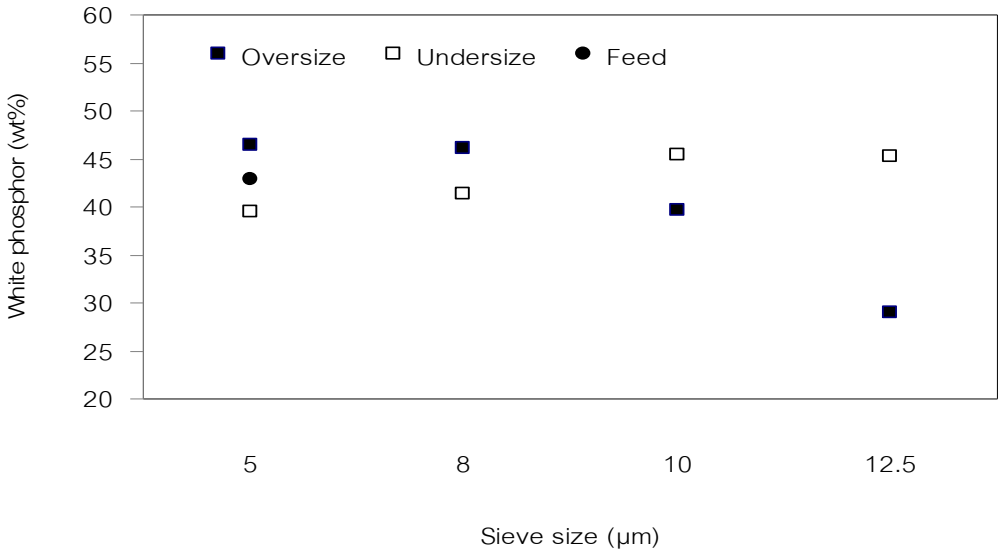

Figure 4.21 Mass fractions of white phosphor in the yields obtained from different sieves

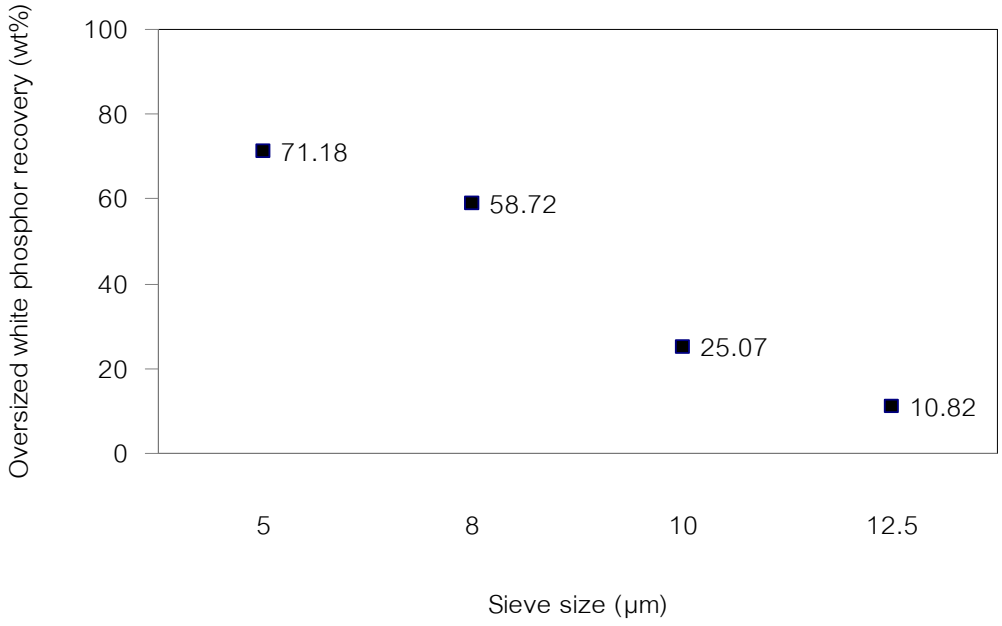

Figure 4.22 Recovery rate of oversized white phosphor.

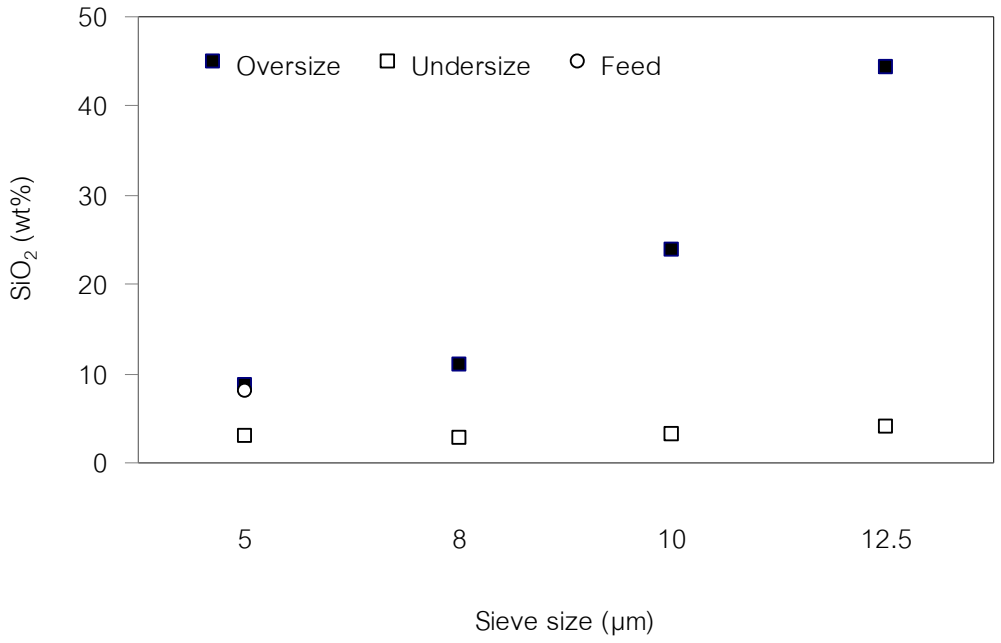

Figure 4.23 SiO_2 impurities in the yields

The amount of glass-impurity could be evaluated from quantitative analysis of SiO_2 in the yields. The mass fraction of SiO_2 in the yields was shown in Figure 4.23. Interestingly, mass fractions of SiO_2 in undersized yields were only about 3%, regardless of sieve aperture size. This indicated that single sieving could separate SiO_2 effectively. The capabilities of the process were highlighted when small sieves opening were employed. Figure 4.24 shows that the recovery rates were higher than 80 wt% in the cases of 5-μm and 8-μm sieves.

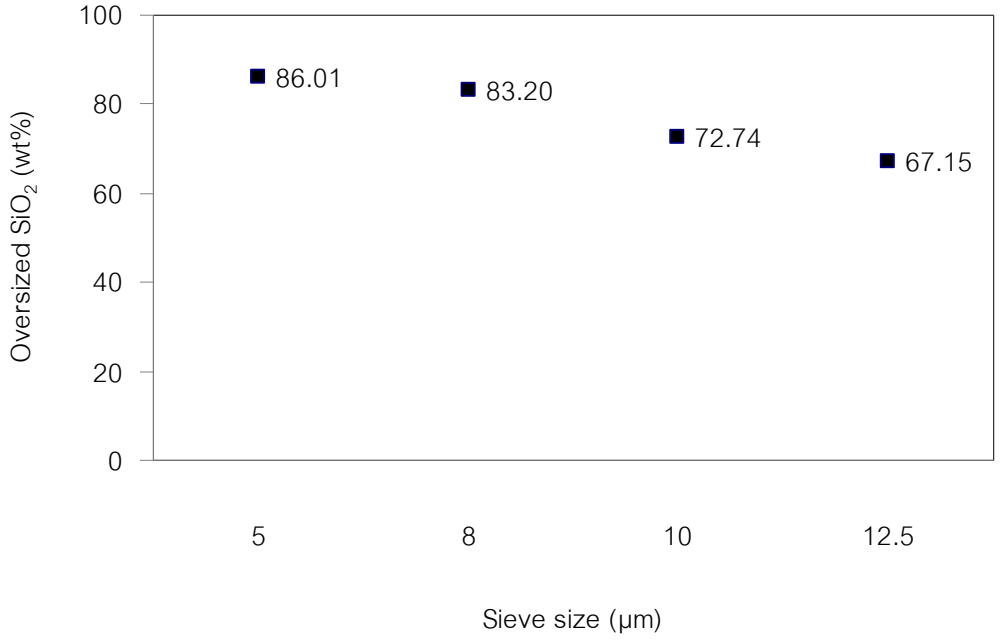

Figure 4.24 Recovery of SiO_2 from oversized yield

Newton's efficiencies of ultrasonic single sieving were evaluated from the recovery rate of rear earth element and were summarized in Figure 4.25. At 5 and 8 μm, Newton's efficiencies were not much different from each other (0.128-0.132). When sieve aperture became larger, the value of Newton efficiency became much lower (0.105 for 10- μm and 0.069-μm). In overall, Newton's efficiency increased when sieve opening size was smaller. From the results, it was suggested that a 5-μm sieve was more suitable than others for a better white-phosphor-separation capability.

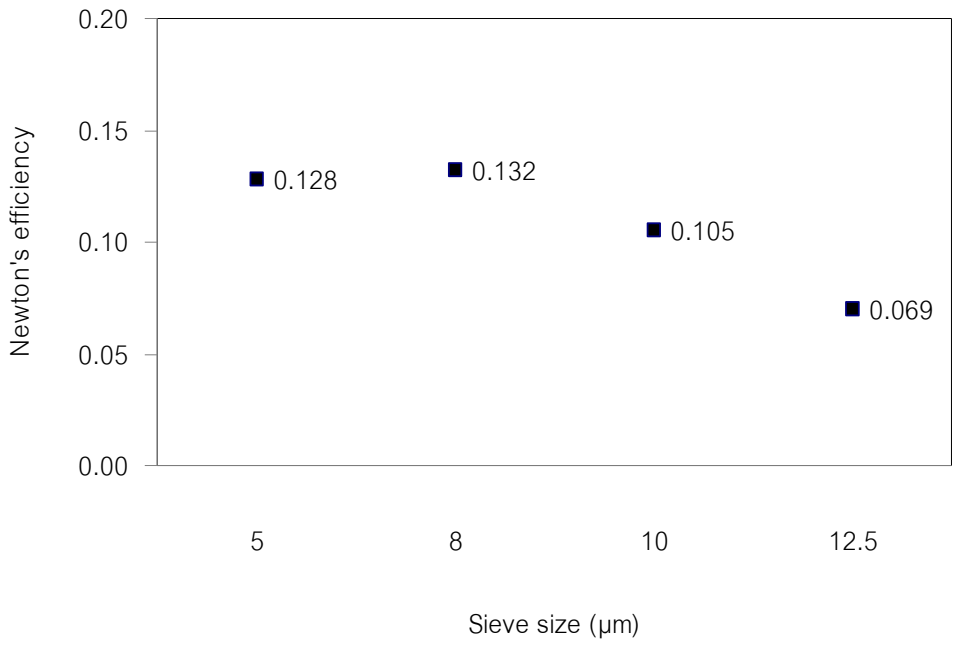

Figure 4.25 Newton's efficiency

4.2 Wet Sieving

Wet sieving is a separation process that is quite similar to dry sieving process except water is additionally fed during the operation. For fine powders, a wet sieving process is considered suitable because dispersion of the fine particles in liquid is easier. (Hidaka and Miwa, 1979). Moreover, electrostatic effects and other agglomerating forces can be reduced. However, the following difficult problems can arise along with utilizing liquid as dispersing medium (Hidaka and Miwa, 1979):

(1) Resistance due to fluid flow of sieve considerably increases,

(2) Resistance due to surface tension of fluid through sieve arises, and

(3) Resistance to fluid flow due to fine particles on the sieve themselves.

Thus it is necessary to investigate a quantitative relationship between these resistances and the aperture dimensions of the sieve.

Resistance to fluid flow of sieve has been previously investigated by Armour and Cannon (1968). Following equation is proposed by treating the sieve as a very thin packed bed:

$$\Delta P_f = f\left(\frac{\rho\left(\frac{U}{E}\right)^2}{g_c} \cdot \left(\frac{L}{D}\right) \right) \tag{4.5}$$

where ΔP_f is pressure drop through the sieve, *f* is the friction factor (f = 8_61/Re + 0.52), ρ is the fluid density, *U* and μ are the velocity and viscosity of fluid, *E* is void fraction of the sieve, Re is the Reynolds number $(\mathrm{Re} = \frac{\rho u L}{\mu})$, *D* is the aperture dimension of sieve, *a* is surface area per unit volume of sieve wire and *L* is fluid path length.

Sieve analysis will normally give information about particles greater than 50 pm in size although meshes down to 5 pm are now available (Robertson et al., 1984). The technical factors which affect the size distributions can be obtained by sieve analysis. Efficient sieving of any sample relies on the arrival of single particles at the sieve apertures. This is a serious potential problem with soil samples due to the formation of groups of particles or aggregates. Soil aggregates are formed firstly in the field where physical shrinkage phenomena associated with wetting, drying, freezing and thawing processes have been shown to be important (Allen, 1981).

In this study, 5-μm sieve opening was used according to an optimum condition obtained from ultrasonic single sieving experiment. Effects of sieving time on the yields and recovery rate were extensively investigated.

4.2.1 Instrument

1. Vibration Sieving Machine (Tsubaki, DK004AM, Japan)

Figure 4.26 Wet sieving

2. 5-μm sieve opening (Tsutsui, 20AT, Japan)

3. FRITCH Water pressure

4. X-ray fluorescent spectrometer

4.2.2 Experiment

Similar to ultrasonic sieving the mixtures were separately poured on to the top of the sieve stack. Any particles remaining in the tubes were rinsed out using clean water. The stack was fitted wit I; the wet sieving attachments supplied by Endecott. This includes a perspex top cover with a hole and a bottom stainless steel drainage plate to which tubing was attached. Vibration amplitude was set at 3 mm based on optimum condition from Chapter III. 20 g of mercury-free used phosphor was used in each batch. Water was added as a fine spray through the top cover 600 ml/min. One litre of distilled water was added as a fine spray through the top cover, during which time the sieve stack was shaken. Normally all the water was added after 4 min with a total of 10 min shaking. After sieving, the samples were dried at 100°C for 8 hours. Undersized and oversized yield mass were recorded. Then, samples were pulverized in a mortar for 30 min in order to perform an elemental analysis using a X-ray fluorescence spectrometer. Thereafter, quantity of each element was determined using predict equation 2.1-2.5 in Chapter III.

The water containing all the particles which had passed through the 63 pm sieve, was collected at the bottom of the sieve stack. The sieves were dried at 90°C and soil particles removed using a sieve brush. After allowing equilibration to room temperature the soil fractions were weighed. (Robertson et al., 1984).

4.2.3 Results and Discussion

- Yield

Table 4.5 shows effect of sieving time on oversized and undersized yields. Figure 4.28 shows a re-plot of oversized and undersized product for visualization purpose. Undersized yields became higher with longer sieving time. The rate of an increase of undersized product was relatively high in the first 10 min of sieving (from 38% at the 1st min to about 80% at the 10th min). The rate of an increase of undersized product was then slower from the 10th to 20th min. At the end of process (the 20th min), undersized yield was 87.3% yield (or 12.7% oversized yield).

Compare to ultrasonic single sieving under the same condition (5-μm sieve, 10 min), only less than 33% yield was obtained. Compare to wet sieving, the same amount of undersized yield was achieved since the 1st min of the operation. A significant improvement of separation capability of wet sieving was due to an ability of water as a dispersive agent thus facilitated the movement of fined particles down through the sieve.

Table 4.5 Effect of sieving time on oversized and undersized yields in wet sieving using a 5-μm sieve opening from 1-20 min

Time (min)	Feed mass (g)	After (g)	Before (g)	Oversized sample retained (g)	Oversized yield (wt%)	Undersized yield (wt%)
1	20	260.51	248.11	12.4	62.00	38.00
2	20	649.39	640.54	8.85	44.25	55.75
3	20	479.76	472.85	6.91	34.55	65.45
4	20	612.31	606.75	5.56	27.80	72.20
5	20	607.59	602.73	4.86	24.30	75.70
10	20.3	610.84	606.9	3.94	19.41	80.59
12	20.2	464.59	460.8	3.79	18.76	81.24
15	20	251.76	248.16	3.6	18.00	82.00
17	20	476.76	473.33	3.43	17.15	82.85
20	20	643.66	641.12	2.54	12.70	87.30

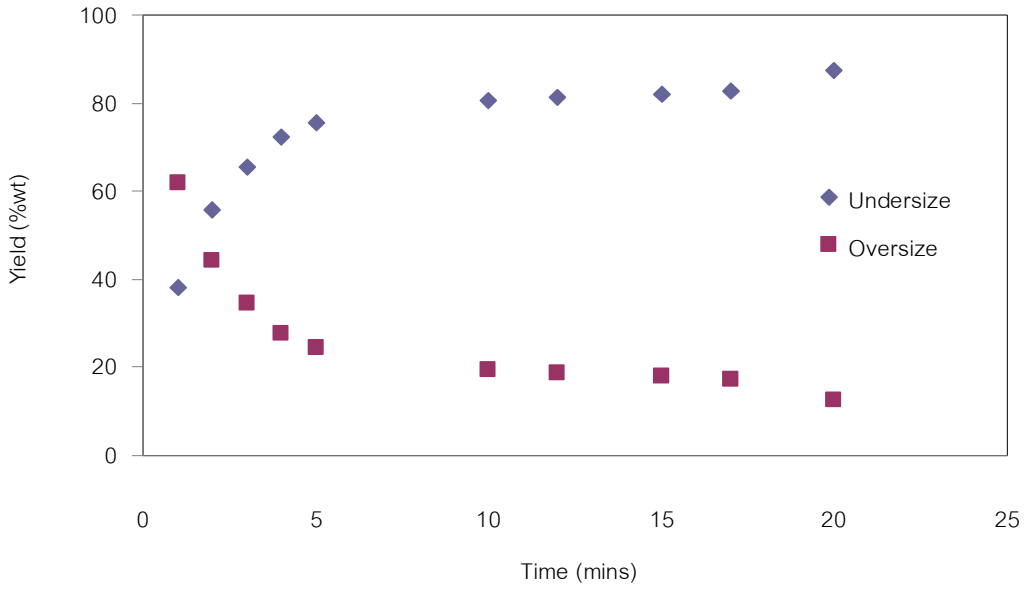

Figure 4.27 Undersized and oversized yields

- Elemental Analysis

Mass fraction of rare earth element in the yield was represented in Figure 4.29. In all cases, the mass fractions of undersized rare earth elements in the yield were much higher than the oversized ones. From the 1st to 5th min of the process, the mass fraction of both undersized and oversized rare earth elements decreased gradually. In the same period, it was observed that the recovery rate of rare earth element increased rapidly from 50% to more than 90% (Figure 4.30). After the 5th min, the recovery rate became quite stable.

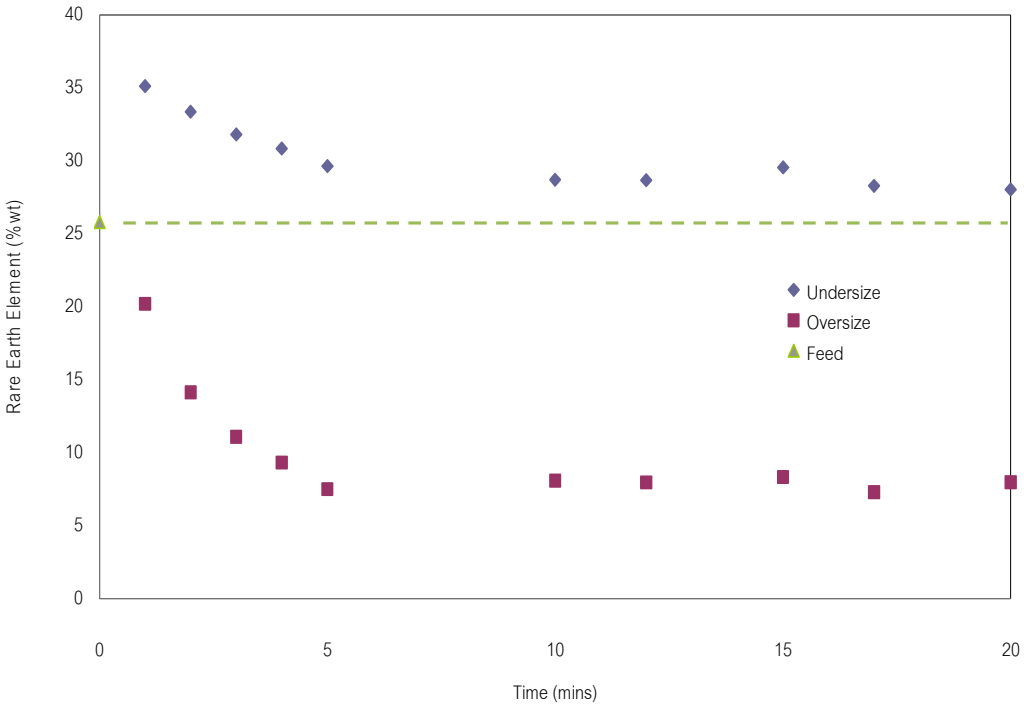

Figure 4.28 Mass fraction of undersized and oversized rare earth elements

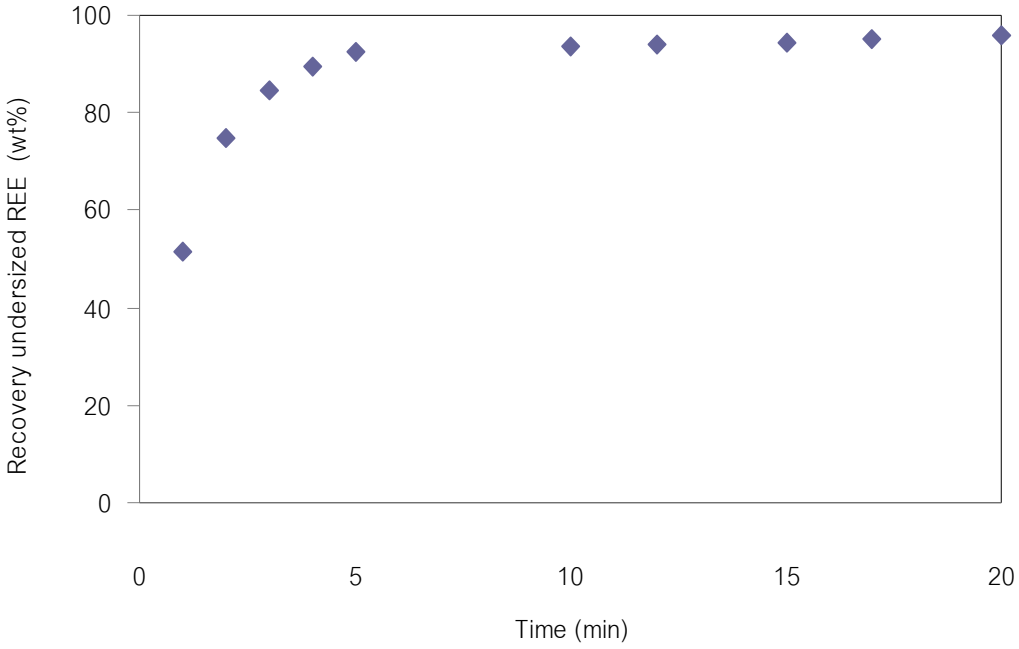

Figure 4.29 Recovery of undersized rare earth element

For white phosphor, undersized particles slightly and gradually increased with sieving time in the first 5 minutes of wet sieving (Figure 4.31). After 5 min, undersized white phosphor was slightly higher than oversized white phosphor. This could be due to the main component CaO dissolved more in water with longer time thus particles of white phosphor could pass the sieve opening. However, this difference was not much. From the 10th min both the mass fraction of undersized and oversized white phosphor particles in the yields became quite constant at the same value of the initial value in the feed. Figure 4.32 shows that oversized white phosphor decreased rapidly from about 70% at the 1st min to about 20% at the 5th min.

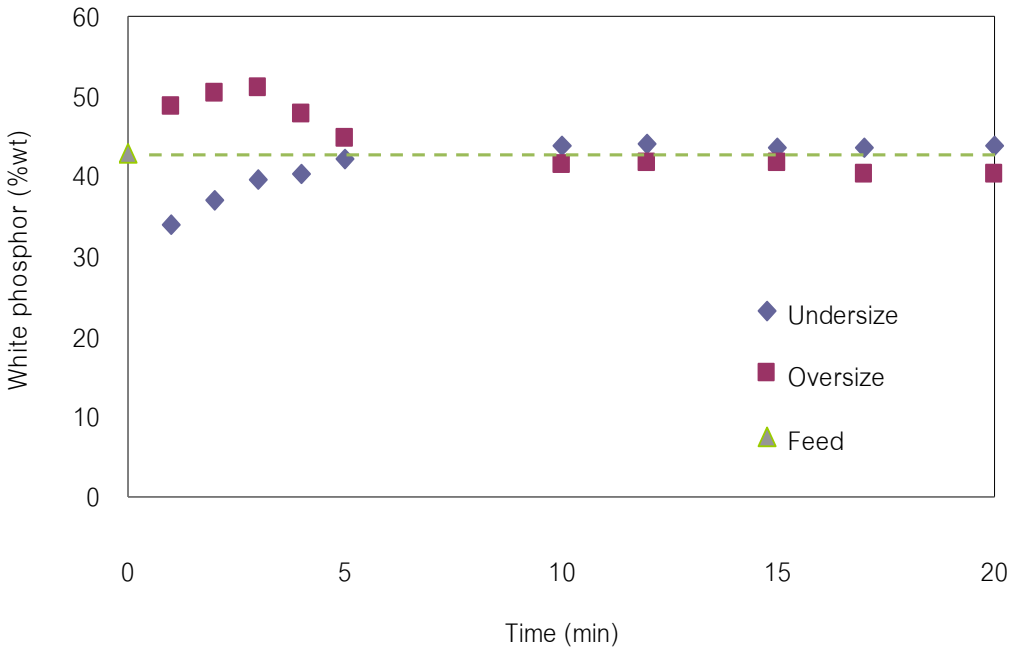

Figure 4.30 White phosphor's mass fraction in the yield obtained after wet-sieving

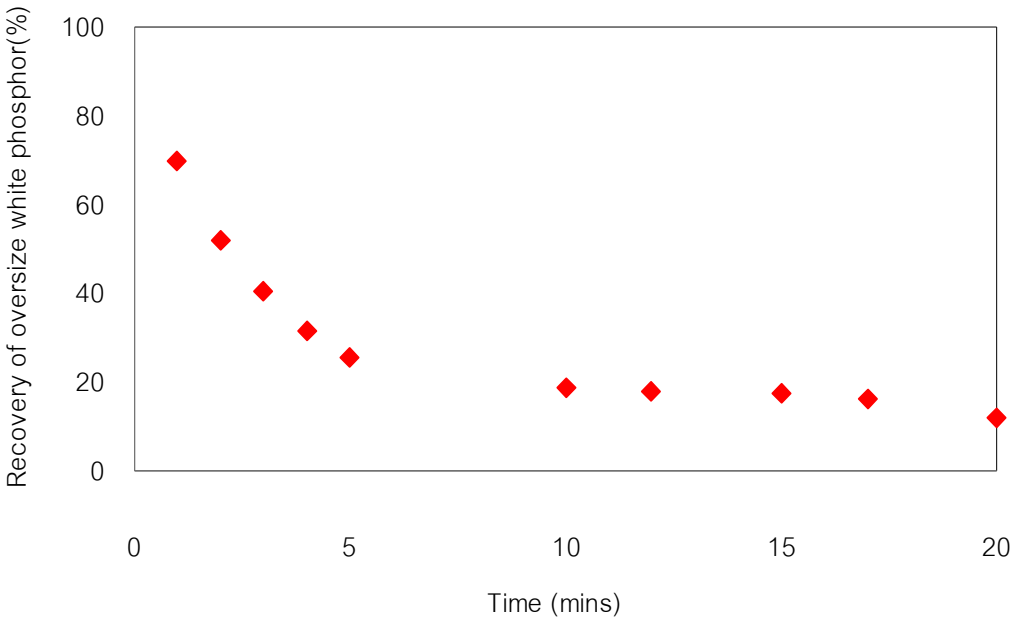

Figure 4.31 Recovery of oversized white phosphor against wet-sieving time

The mass fraction of SiO_2 in the yield was shown in Figure 4.33. Similarly to ultrasonic single sieving, undersized SiO_2 in the yields obtained from yields were less than 4%, no matter the sieving time was. This indicated that wet sieving could also effectively separate SiO_2. Figure 4.34 shows the recovery rate of SiO_2. Recovery rate slightly decreased with sieving time.

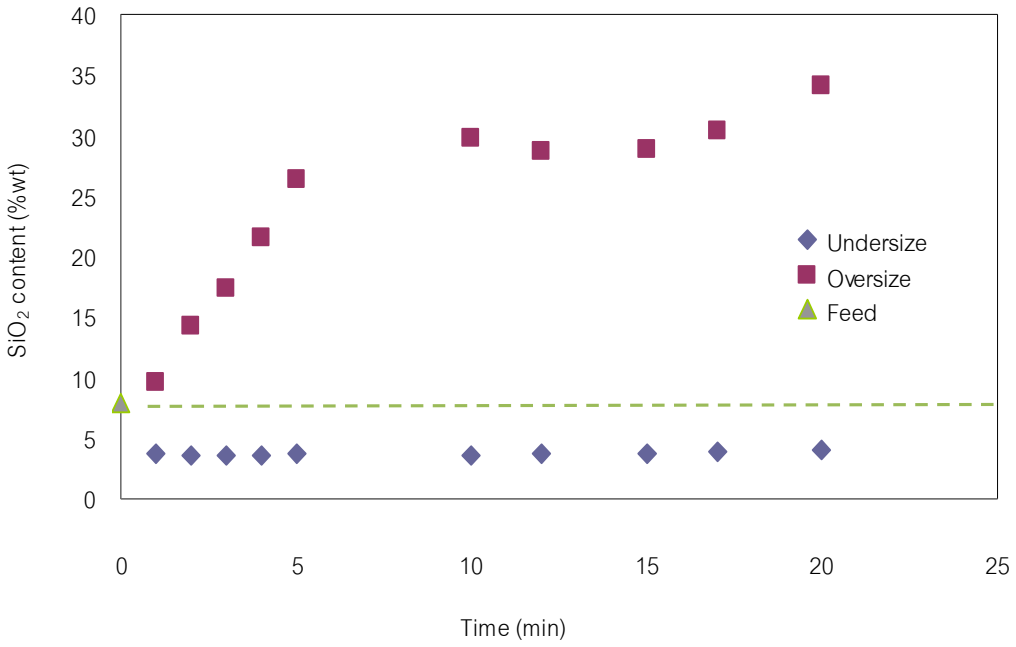

Figure 4.32 SiO_2 impurities's mass fraction in the yield obtained after wet-sieving

Lastly, Newton's efficiency of wet sieving was evaluated (Figure 4.35). At the 2nd min of the sieving the highest value of Newton's efficiency of 0.254 was achieved. This value of Newton's efficiency was much higher compare to ultrasonic single sieving. Increasing sieving time could decrease Newton's efficiency. The lowest Newton's efficiency was fond at the longest sieving time. As a conclusion for this subsection, it seemed that wet sieving could reduce process time compared to dry sieving. However, too long sieving time might have a negative effect in term of a decreased in the recovered oversized-white-phosphor and oversized-SiO_2 (or glass), or in another word, undersized impurity in the undersized yields would increase with wet-sieving time.

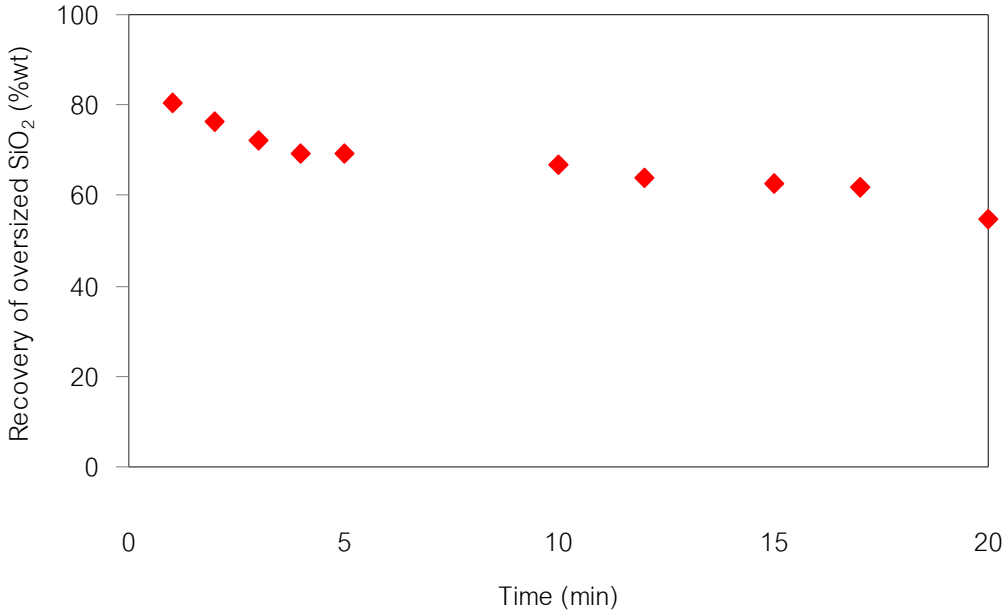

Figure 4.33 Recovery of oversized SiO_2 against wet-sieving time

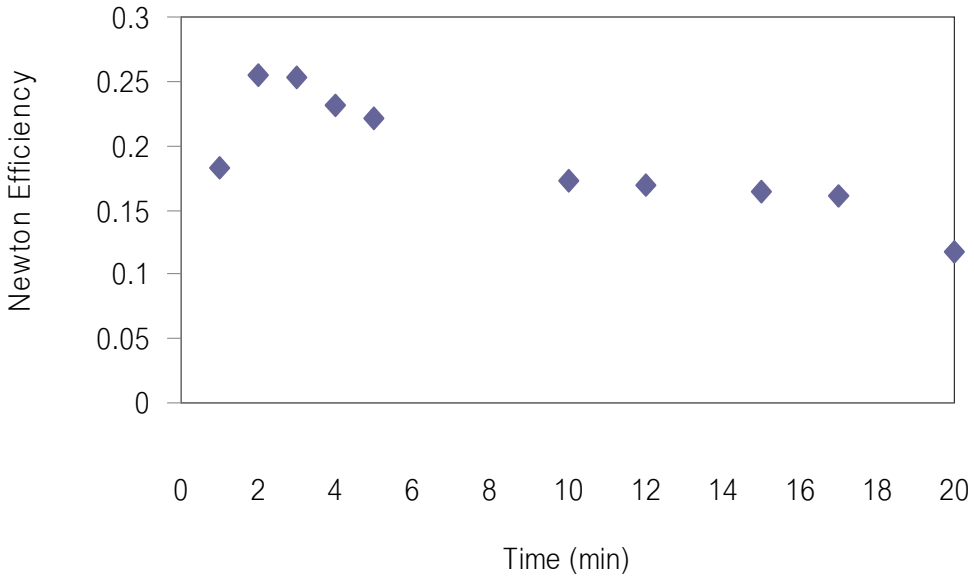

Figure 4.34 Newton's efficiency

4.4 Air Classification

Air classification is a dry-state classification method which separates the powder using air flow. Up to now, dynamic-state air classifiers have been developed in the form of the third generations, with and cyclone classifiers as the first and second generations, respectively (Duhamel et al, 1997).

Compared to its predecessors, the first advantage of turbo air classifier is the employment of the rotor cage as the classification component which can exert a radial forced centrifugal field. Another advantage is that the air flows into the classifier in the tangential direction then it is directed by the guide vanes, forming a uniform field in the classification region. After powder material is fed through the upper feed port and is thrown outward by rapidly rotating the distribution plate, it drops into the classification region. This arrangement is favorable for the dispersion and separation of the powder material. Thus, turbo air classifier can achieve high classification performance (Guo et al., 2007).

Powder material to be classified is fed through the feed material entrance and falls to the distribution plate. By rapidly rotating the distribution plate, the powder on it is thrown outward then dropped into the annular region. Under influences of the air currents and rotation of the rotor cage the materials is divided into coarse and fine powders (Liu et al., 1997). There are two dominant forces acting on the particle along the radial direction in the classification region, e.g. the inertia centrifugal force and the fluid drag force. When the rotor cage rotates, the inertia centrifugal force is created. The fluid drag force results from the exposure of particles to the air flow pumped by the fan (Jiaxiang Liu et al., 2003). It is assumed that tangential and radial velocity in the circumferential and vertical directions are uniform and particles are spherical. The equation of motion of a single particle in the annular region is given by (Morimoto et al., 2003) as shown below:

$$m\frac{DV_{pr}}{Dt} = F_D + F_C \tag{4.6}$$

$$F_D = \frac{1}{2}C_D(\mathrm{Re})\rho_a(V_{pr} - V_r)\left|V_{pr} - V_r\right|\frac{\pi}{4}d^2 \tag{4.7}$$

$$F_C = m\frac{V_\theta^2}{r} = \frac{1}{6}\pi d^3\rho_p\frac{V_\theta^2}{r} \tag{4.8}$$

where F_D is the fluid drag force towards the rotor cage center and F_C is the inertia centrifugal force opposite to F_D.

It is assumed that there is no slip between particle and air tangential velocity. When the centrifugal force and fluid drag force reach equilibrium on the particle at the outer periphery of the rotor cage, and if the radial velocity of the particle is zero, the size of the particle is called cut size, d_{50}, which can be expressed as follows: ??

$$d_{50} = 3C_D\rho_a r V_r^2 / 4V_\theta^2\rho_p \tag{4.9}$$

From the equation above, it can be seen that the value of the cut size is not fixed, and it changes in a certain range (Wang et al., 1998). Drag coefficient, C_D, is a function of the Reynolds number which is further related to the air velocity and other factors, i.e. density and viscosity. For a given powder material, when particle and air density are constants, d_{50} is primarily dependent on the radial and tangential velocities. Consequently, it can be seen from Equation 4.9 that decreasing the ratio of V_r to V_θ should give a smaller cut size.

Figure 3.36 shows the schematic diagram of an air classifier manufactured by Hosokawa (Micron 200TSP, Japan). Samples will be fed from the top of the classifier. While passing through the air classifier, the particles will experience centrifugal force and inertia force. The particles having larger diameters (coarse powder) are discharged

from the outside with large centrifugal force while small particles (fine powder) are discharged from the inner diameter with lower centrifugal force.

In this study, air classification from centrifugal wind was employed. The coarse (underflow) and fine (overflow) particles were expected to be separated due to difference centrifugal forces. Concentrate of rare earth element representative in fine particles, glass and white phosphor are coarse particles.

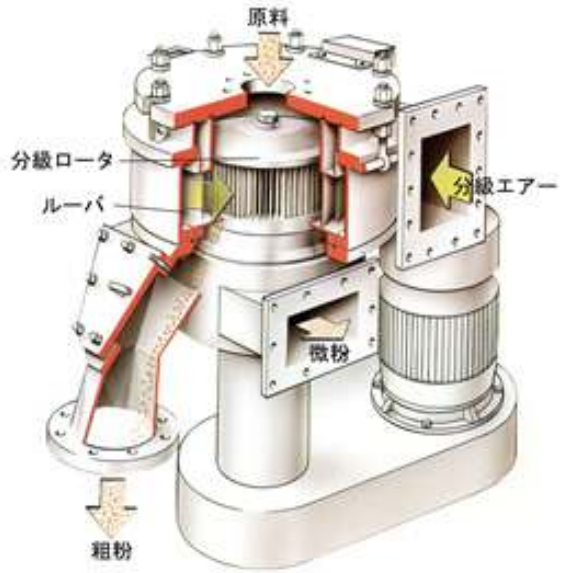

Figure 4.35 Air classifier

4.4.1 Instrument

1. Air classifier (Hosokawa Micron, 200TSP TSP, Japan)

2. X-ray fluorescent spectrometer

4.4.2 Experiment

Figure 4.37 shows a work-flowchart of an air classifier. Samples were fed to the classifier by a screw feeder. Compressed air might be additionally supplied for at least two purposes: to adjust feed rate and to disperse the particles that were in an aggregated form before the classification. The samples were then separated into coarse powder and fine powder forms. The coarse powder was removed while fine powder was collected using a cyclone and dust collector in next step.

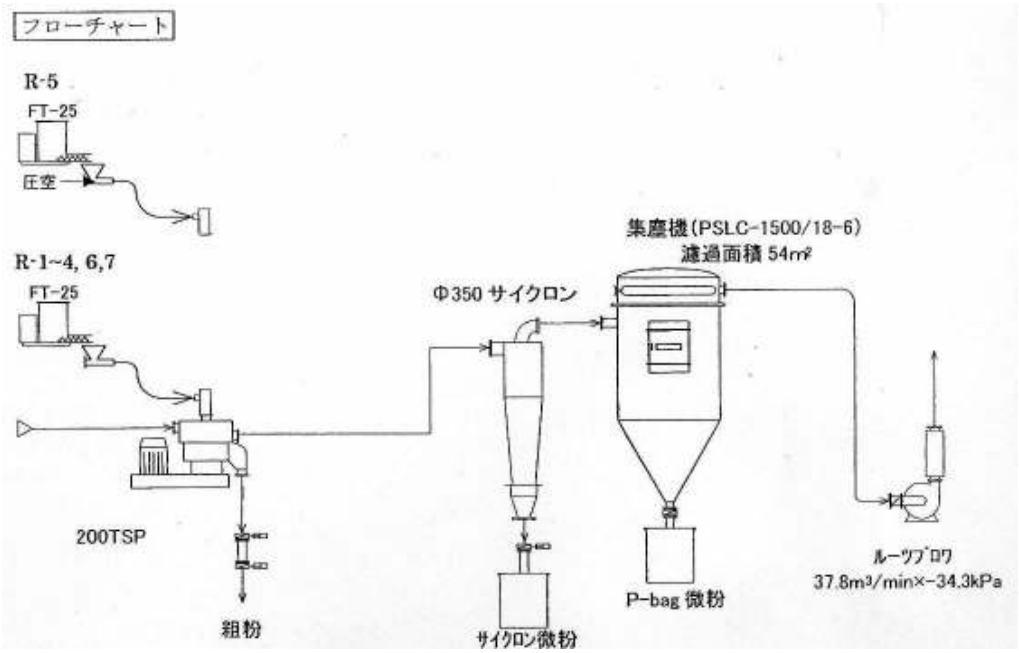

Figure 4.36 Flow chart of model experiment

The feed rate of used sample was set at 60 kg/h with no additional compressed air. Rotation speeds of 2000, 3000, 4000, 5000 and 6000 rpm were tested. For a comparison purpose, at only a rotation speed of 3000 rpm the feed rate of 120 kg/h with

no compressed air and 60 kg/h with compressed air supply were also tested. All the experiment's conditions and the obtained fine and coarse yields were summarized in Table 3.5. After the process, coarse and fine powders were separated. Each sample was pulverized in a mortar for 30 min. The sample was then elemental analyzed using an X-ray fluorescence spectrometer in the same way described before. Predicted equations (equation 3.1, 3.2, 3.3, 3.4 and 3.5) were used for quantitative analysis of rare earth element, white phosphor and glass.

Table 4.6 Yields obtained from air classification at different conditions

Run No.	1	2	3	4	*5	6	7
Feed rate (kg/h)	60	60	60	60	60	60	120
Rotational speed (rpm)	6000	5000	4000	3000	3000	2000	3000
Fine yield (%)	8.6	10.4	15.8	24.6	34.6	56.4	20.6
Coarse yield (%)	91.4	89.6	84.2	75.4	65.4	43.6	79.4

* *With compressed air*

4.4.2 Results and Discussion

- Yield

Figure 4.38 shows the overflowed yield or fine particles. Higher overflowed yields were obtained at lower rotational speed. As mentioned above three conditions were used at a rotation speed of 3000 rpm: a) feed rate of 60 kg/h no compressed air; b) feed rate of 60 kg/h with compressed air; and c) feed rate of 120 kg/h no compressed air. Under condition (a) the obtained yield was 24.6 wt%. The yield was boosted up to 34.6 wt% when compressed air was additionally supplied at the same feed rate (condition (b)). This was due to the ability of compressed air to disperse aggregated particles. However, at condition (c) the overflowed yield was reduced to about 20 wt%. An increasing in the feed rate might reduce resident time of particles in the working chamber and the alignment of particles became denser, thus reduced separation's efficiency. At the maximum rotational speed the overflowed yield was reduced to only about 9 wt%, the fact indicated that a using of too high rotational speed reduced an overflowed yield and should be avoided.

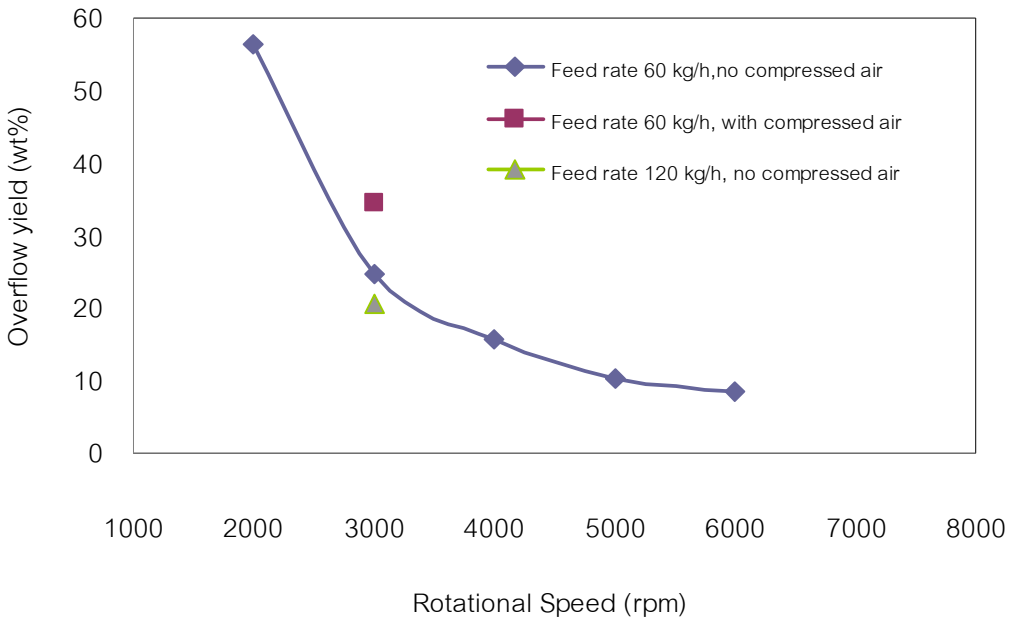

Figure 4.37 Overflowed yields (fine particles) at different rotational speeds

- Elemental Analysis

Before classification, the mass fraction of rare earth elements in the feed was 25.79 wt%. Figure 4.39 shows rear earth element contents in the coarse powder (underflow) and fine powder (overflow) after air classification. Clearly, air classification at a rotational speed of 3000 rpm offered maximum rear earth element contents in fine powder of 43.26 wt%. Beyond this optimum speed, the mass fraction of rear earth element began to decline with an increasing of rotational speed. The minimum mass fraction of rear earth element was found as 8% at the maximum speed of 6000 rpm.

A maximum recovery rate of rare earth element was found to be 80.34 wt% at the lowest rotation speed of 2000 rpm and sharply reduced to 41.48 wt% at 3000 rpm. The recovery rate sharply increased to 59.21 wt% when compressed air was additionally

supplied. Therefore, by providing compressed air to disperse the particles agglomerated particles could affect the recovery rate of rare earth element. In contrast, increasing the feed rate to 120 kg/h at the same rotational speed decreased recovery rate to 34.32 wt%. Further increase rotational speed to 4000, 5000 and 6000 rpm continuously reduced recovery rates of rare earth element to 25, 14 and 11 wt%, respectively.

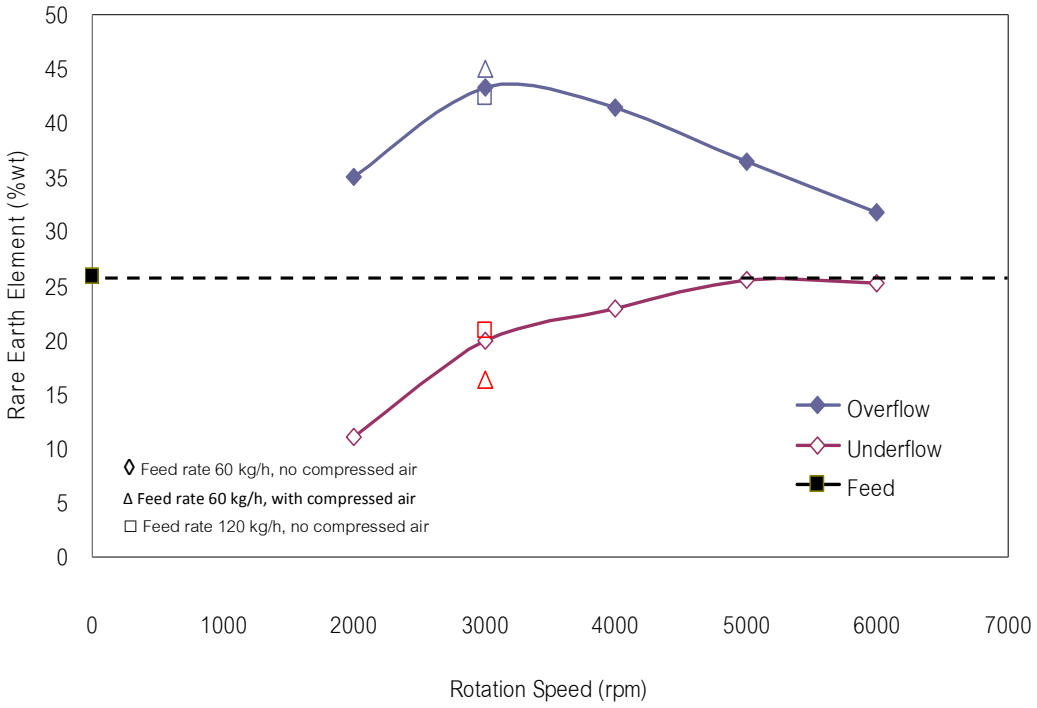

Figure 4.38 Rare earth elements content in the yields obtained from air classification

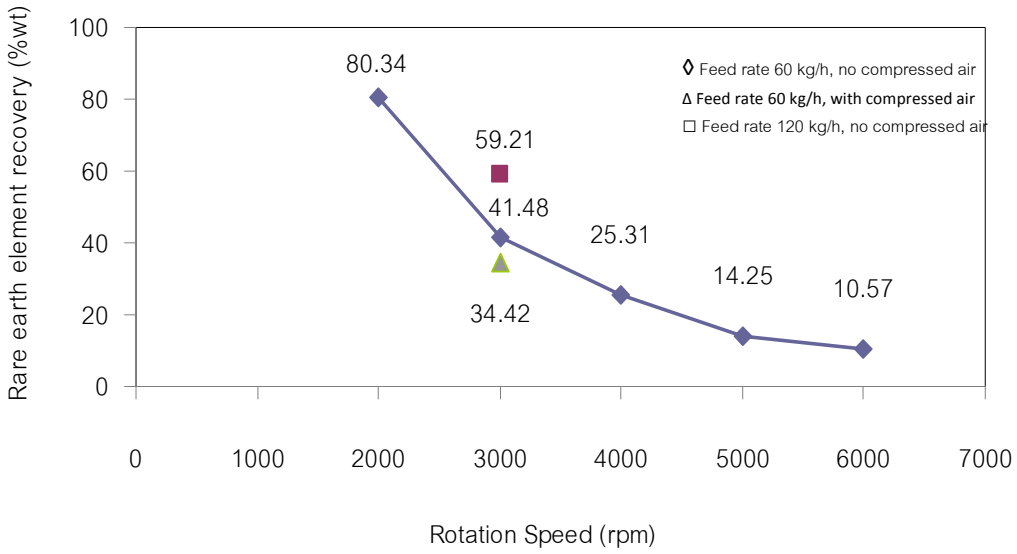

Figure 4.39 Rare-earth-element recovery rates in underflowed yields

Figure 4.41 shows the effects of rotational speed on white phosphor content in the yields. In general, mass fractions of white phosphor in underflowed yields were much higher than mass fractions of white phosphor in overflowed yields. Maximum white phosphor content in underflowed particles of 59.14 wt% was obtained at the lowest rotational speed. White phosphor content in overflowed particles (fine powder) decreased to the minimum value of 17 wt% at a rotation speed 3000 rpm. This implied that the rotation speed of 3000 rpm could be an optimum condition to performed separation white phosphor from the fine powder. Compressed air and feed rate showed little effect on mass fractions of white phosphor in both overflowed and underflowed particles.

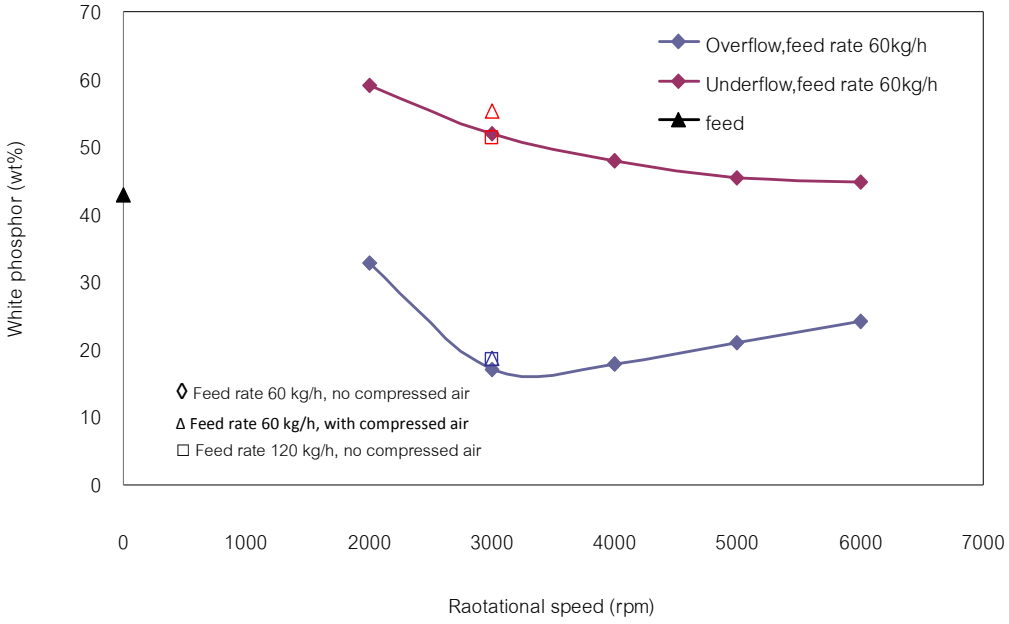

Figure 4.40 White phosphor contents in the yields obtained from air classification

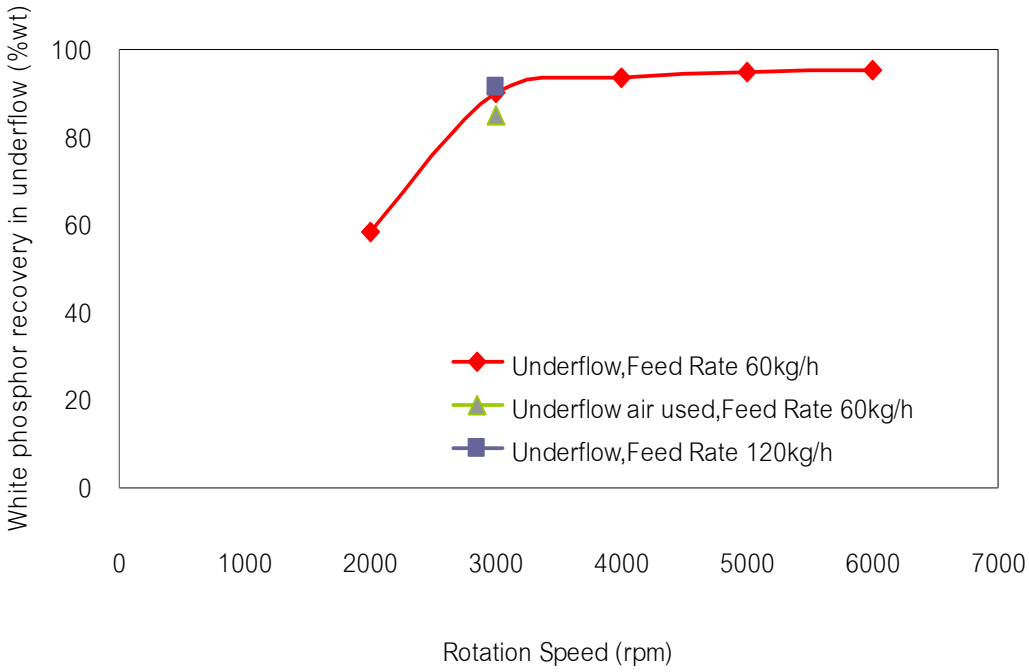

Figure 4.41 White-phosphor recovery rates in underflowed yields

Figure 4.43 shows the effects of rotational speed on SiO_2 impurities in overflowed and underflowed particles. Before classified SiO_2 impurities was about 8 wt%. After classified at a rotation speed of 2000 rpm, maximum SiO_2 impurities of 11.10 wt% in underflowed particles was found. At a rotation speed of 3000 rpm and flow rate of 60 kg/h with no compressed air, SiO_2 impurities in oversized and undersized products were 7.05 and 7.63 wt%, respectively. When compressed air was additionally supplied, SiO_2 contents in oversized product (fine particle) reduced to 6.28 wt% while SiO_2 contents in undersized product (coarse particle) increased to 8.96 wt%. At the same speed, increasing feed rate to 120 kg/h showed little effect on SiO_2 content in both oversized and undersized particles (6.87 and 6.91 wt% respectively). At higher rotational speed of 4000, 5000 and 6000 rpm, SiO_2 content in an overflowed yield became higher than SiO_2 content in an underflowed yield, which meant that fine particle were more contaminated by glass than coarse particle was.

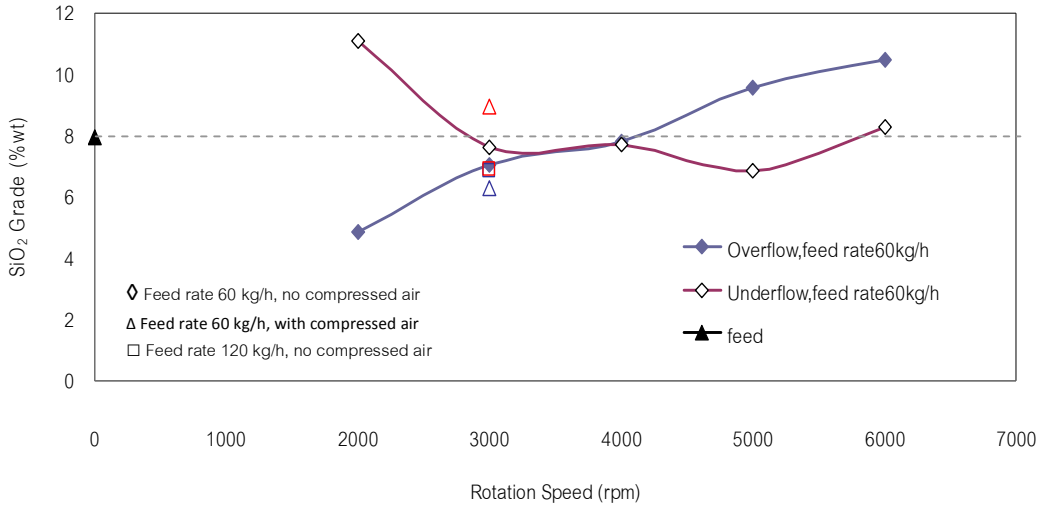

Figure 4.42 SiO_2 impurities in the yields obtained from air classification

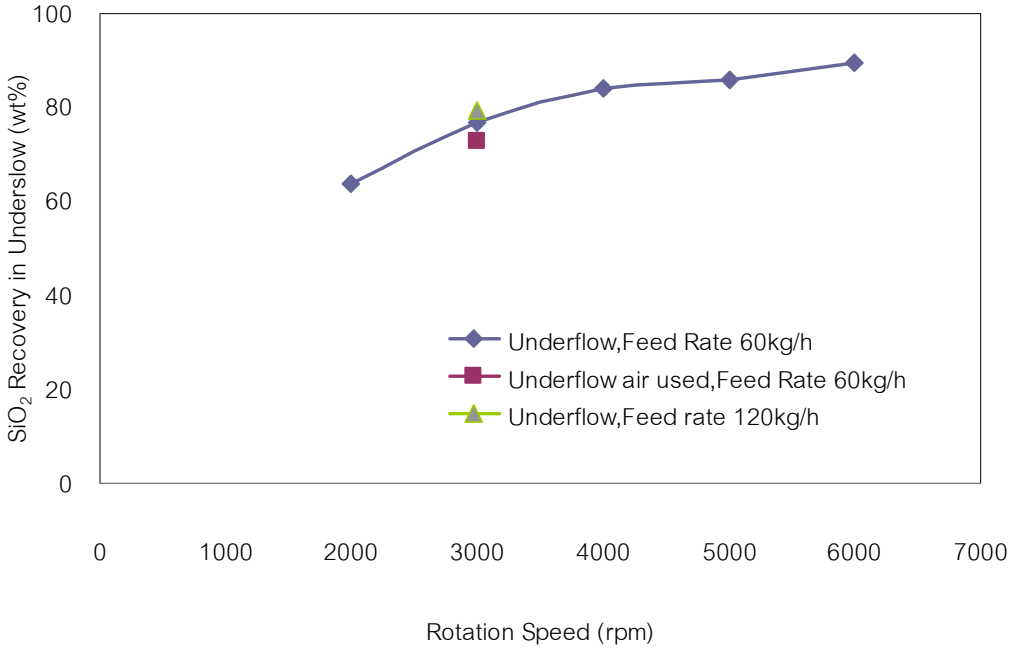

Figure 4.43 SiO_2 recovery rates in underflowed yields

In Figure 4.44, relationship between rotational speed and recovery rate of SiO_2 from underflowed yield was presented. It was found that increasing rotational speed raised the recovery rate of SiO_2. At 3000 rpm, when compressed air was not used, the recovery rate of SiO_2 was 76.84 wt%. The recovery rate was slightly decreased to 72.95 wt% when compressed air was used but slightly increased to 79.49 wt% when feed rate was increased to 120 kg/h. The compressed air has a significant to improve removal glass and obtained high grade in the same rotation speed 3000 rpm except for increase feed rate.

Lastly, Newton's efficiency estimated from percentage of separation was summarized in Figure 3.46. When no compressed air was used, Newton's efficiency became as high as 0.29 at a rotation speed of 2000 rpm. By the way, when compressed air was additionally supplied at a rotational speed of 3000 rpm, Newton's efficiency increased to a maximum value of 0.34. The classification capability was noticeably improved with the use of compressed air.

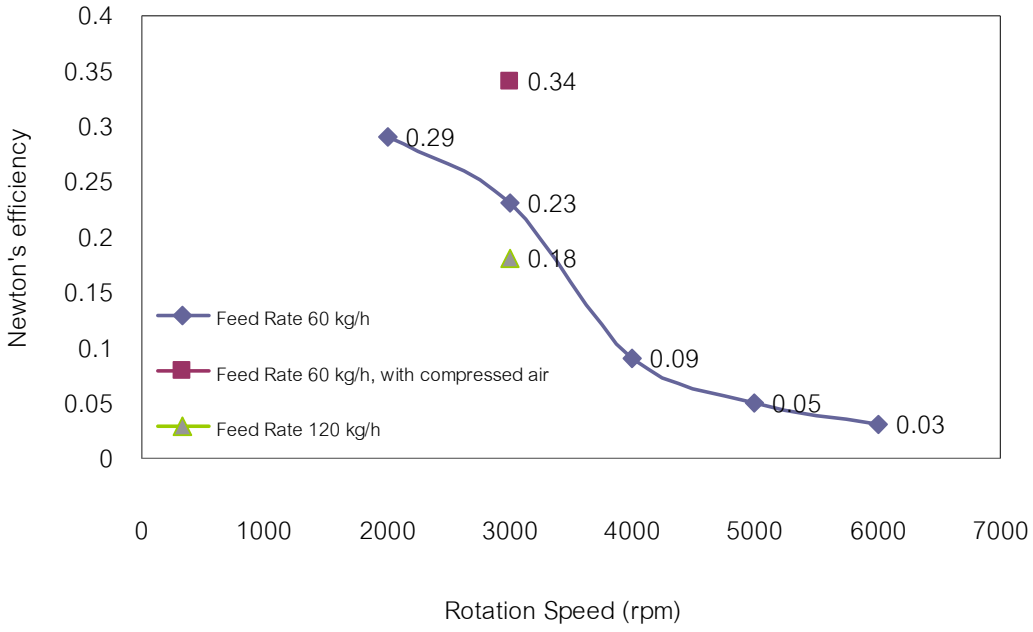

Figure 4.44 Newton's efficiency

CHAPTER IV

CONCLUSION

5.1 Discussion

5.1.1 Sample's characterization

In the first part, elemental analysis showed that fresh phosphors contained various oxides of rare earth element. Rear earth elements were found only in red (Y_2O_3 and Eu_2O_3), blue (Y_2O_3 and Eu_2O_3), and green (La_2O_3, CeO_2 and Tb_4O_7) phosphors while white phosphor contained none of rare earth element but only CaO. All calibration curves developed to predict the quantity of rear earth elements in the fresh (and also later in the used) samples exhibited strong linear relationships between mass fraction of element and mass of phosphors or glass in the bulk with R^2 higher than 95% for every case. Elemental analysis of used phosphors confirmed that mercury-free used phosphors contained rare earth elements. Thus mercury-free used phosphor was used as a representative for used phosphor in separation processes. Glass was also mixed in the used phosphors in order to mimic the used fluorescent-lamp industrial waste.

Results also revealed that there were differences among the sizes of impurities (glass and white phosphor) and rear earth elements. Thus it was reasonable to apply physical separation methods to separate rear earth elements from the used samples.

5.1.2 Dry Sieving

In normal vibration sieving, agglomeration among small particles extensively took place as confirmed by the fact that most of particles could not passed through the 10-μm sieve opening. The formations of bigger particles finally lead to clogging. The maximum vibration amplitude used in this experiment (3 mm) was found to be insufficient to disperse aggregated particles. Thus low yields were obtained, regardless the vibration amplitude was.

To overcome the problem in normal vibration sieving, ultrasonic sieving was employed with the expectation that yield and rear earth element could be improved. When ceramic balls were mixed with the samples, yield's mass of smaller particles became relatively high. This confirmed the capability of ultrasonic sieving with dispersive agent to enrich rare-earth-element contents. Sieving time had an impact on the mass ratio of the yields that were smaller than 10 μm and the best result obtained when total sieving time was 10 min. The separation of SiO_2 was found to be quite effective even after using only a 20-μm sieve. Nevertheless, white phosphor still contaminated with rare earth elements on the smaller sieves. This could be because several sieving layers resulted in over-vibration to white phosphor particles thus broke such particles into small pieces. Finally, the optimum condition of the single ultrasonic sieving was: sieve opening = 5 μm and sieving time = 10 min. At the optimum condition, Newton's efficiency was 0.128.

5.1.3 Wet Sieving

Based on the results obtained from dry sieving experiment, Newton's efficiency of wet sieving was investigated. A 5-μm sieve was used but with different sieving times (1, 2, 3, 4, 5, 10, 12, 15, 17 and 20 min). The highest Newton efficiency were obtained when sieving times were 2 and 3 min. However, white phosphor impurity in the yields was found to higher with longer shaking time. When white phosphor separation capability was considered, the optimum condition for wet sieving could be found as: sieve aperture = 5 μm and sieving time = 2 min. Maximum Newton's efficiency was 0.254.

5.1.4 Air Classifier

Lastly, effects of rotor speed and compressed air in air classification on separation efficiency were investigated. The best condition was found when the rotation speed was 3000 rpm with compressed air. At this condition, quantity of white phosphor in overflow was lowest (less than 20 wt%) and the recovery of white phosphor was more than 80 wt%.

5.2 Comparison of Newton's efficiency of each sieving method

The values of Newton's efficiency obtained from ultrasonic single sieving, wet sieving and air classification at the optimum condition of each process were summarized as shown in Table 4.1. The mentioned optimum condition was selected from 1) the recovery rate of rear earth element and 2) the capability of the process to separate impurities from undersized products. Ceramic balls as a dispersive agent were found to be important in ultrasonic single sieving. In term of process time and the

recovery rate of rear earth element, wet sieving was found to be 5 times faster than dry sieving and offered higher recovery rate. While dry and wet sieving in this experiment were batch processes, air classification was the only one continuous method in this study. Higher separation capacity with extremely high recover rate of rear earth element was possible.

Table 5.1 Newton's efficiencies at the optimum conditions of different separation methods

Method	Newton's efficiency	REE recovery rate (wt%)	Optimum condition
Ultrasonic single sieving	0.13	42	Sieve aperture = 5 μm Sieving time = 10 min With ceramic balls
Wet sieving	0.25	75	Sieve aperture = 5 μm Sieving time = 2 min Water assisted
Air classification	0.34	80	Rotational speed = 3000 rpm Compressed-air assisted Feed rate = 60 kg/h

However, it should be noted here that optimum condition suggested in this report was just only the best condition selected from all conditions that were tested in this study but might be not the actual best condition for the process.

5.3 Recommendation

In overall, the result from this study was found to be practical enough for industrial side. This study was all conducted in Japan as well as the source of raw materials used in the study. The quantity of sample was limited according to its availability. It was suggested that there were some possibilities to conduct the experiment in Thailand in the future if the raw material's source from the industrial plant is available and the design of air classification was suitable. Further investigations that might be of great interest were experiments on new design of air classification machine, the simulation of various feed direction and so on.

References

Apisitpuvakul, W.; Piumsomboon, P.; Watts, J.D. and Koetsinchai, W. LCA of spent fluorescent lamps in Thailand at various rates of recycling Bangkok: Journal of Cleaner Production, 2008.

Asari, M.; Fukui, K. and Sakai, Sh. Life-cycle flow of mercury and recycling scenario of fluorescent lamps in Japan Kyoto: Science of the total environment, 2008.

Berlin, N. Test sieving principle and procedure Wisconsin: The leader in sieving technology, 2001.

Daeschner W.H. Wet sieving with precision electroformed sieves California: Shell development company, 1969.

Guo, L.; Liu, Jiaxiang.; Liu, Sh. and Wang, J Velocity measurements and flow field characteristic analyses in a turbo air classifier Beijing: Powder Technology, 2007.

Hall, S.W. and Beddow K.J. Ultrasonic vibration in sieving London: Research and development, 1969.

Hedrick, B.J. Rare earths Advance release California: Minerals yearbook, 2007.

Hidaka, J. and Miwa, S. Fractional and particle size analysis of fine powders by micro sieve Kyoto: Powder Technology, 1979.

Hirajima, T.; Petrus, H.T.B.M.; Oosako, Y.; Nonaka, M.; Sasaki, K. and Ando, T. Recovery of cenospheres from coal fly ash using a dry separation process: Separation estimation and potential application Kyushu: International Journal of Mineral Processing, 2010.

Hirajima, T.; Sasaki, K.; Bissombolo, A.; Hirai, H.; Hamada, M. and Tsunekawa, M. Feasibility of an efficient recovery of rare earth-activated phosphors from waste fluorescent lamps through dense-medium centrifugation Kyushu: Separation and Purification Technology, 2004.

Jang, M.; Hong, M.S. and Park, k. Characterization and recovery of mercury from spent fluorescent lamps Madison: Waste Management, 2004.

Leschonski, K. and Rumpf, H. Principle and construction of two new air classifiers for particle size analysis Karlsruhe: Journal of Cleaner Production, 1986.

Liu, K. Some factors affecting sieving performance and efficiency Aberdeen: Powder Technology, 2009.

Petrus, H.T.B.M.; Performance of dry-separation processes in the recovery of cenospheres from fly ash and their implementation in a recovery unit Kyushu: International journal of mineral processing, 2010.

Peukert, W. and Wadenpohl, C. Industrial separation of fine particles with difficult dust properties Munich: Powder Technology, 2001.

Rabah, A.M. Recyclables recovery of europium and yttrium metals and some salts from spent fluorescent lamps Cairo: Waste Management, 2007.

Robertson, J.; Thomas, J.C.; Caddy, B. and LBWIS J.M.A. Particle size analysis of soils a comparison of dry and wet sieving techiques Glasgow: Forensic Science International, 1983.

Sivamohan, R. The problem of recovering very fine particles in mineral processing Amsterdam: International journal of mineral processing, 1990.

APPENDICES

Appendix

Analytical machines in this study

X-Ray Fluorescence (XRF) Spectrometry

XRF Spectrometry is used to identify elements in a substance and quantify the amount of those elements present to ultimately determine the elemental composition of a material. An element is identified by its characteristic X-ray emission wavelength (λ) or energy (E). The amount of an element present is quantified by measuring the intensity (I) of its characteristic emission.

All atoms have a fixed number of electrons (negatively charged particles) arranged in orbitals around the nucleus. Energy Dispersive (ED) XRF and Wavelength Dispersive (WD) XRF Spectrometry typically utilize activity in the first three electron orbitals, the K, L, and M lines, where K is closest to the nucleus.

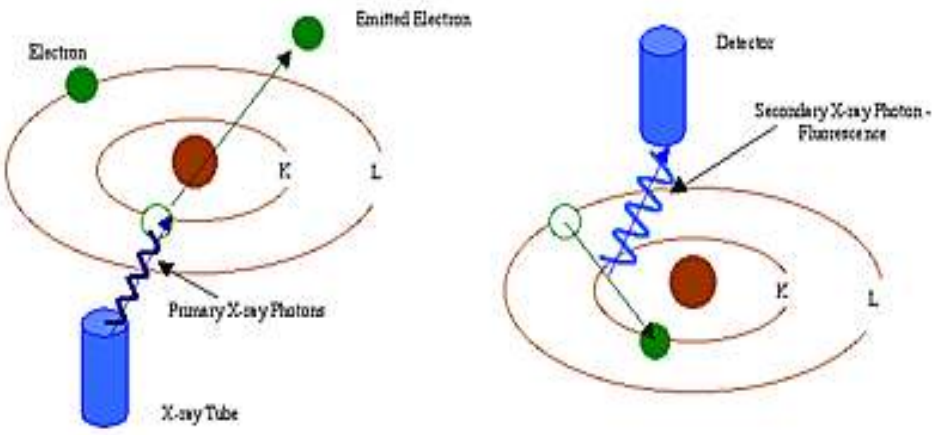

Figure A-1 Schematic of X-ray fluorescence spectrometry

In XRF Spectrometry, high-energy primary X-ray photons are emitted from a source (X-ray tube) and strike the sample. The primary photons from the X-ray tube have

enough energy to knock electrons out of the innermost, K or L, orbitals. When this occurs, the atoms become ions, which are unstable. An electron from an outer orbital, L or M, will move into the newly vacant space at the inner orbital to regain stability. As the electron from the outer orbital moves into the inner orbital space, it emits an energy known as a secondary X-ray photon. This phenomenon is called fluorescence. The secondary X-ray produced is characteristic of a specific element. The energy (E) of the emitted fluorescent X-ray photon is determined by the difference in energies between the initial and final orbitals of the individual transitions.

This is described by the formula

$$E=hc\lambda^{-1}$$

Where h is Planck's constant; c is the velocity of light; and λ is the characteristic wavelength of the photon.

Energies are inversely proportional to the wavelengths; they are characteristic for each element. For example the Kα energy for Iron (Fe) is about 6.4keV. Typical spectra for EDXRF Spectrometry appear as a plot of Energy (E) versus the Intensity (I).

XRF Spectrometry is the choice of many analysts for elemental analysis. XRF Spectrometry easily and quickly identifies and quantifies elements over a wide dynamic concentration range, from PPM levels up to virtually 100% by weight. XRF Spectrometry does not destroy the sample and requires little, if any, sample preparation. It has a very fast overall analysis turnaround time. These factors lead to a significant reduction in the per sample analytical cost when compared to other elemental analysis techniques. Aqueous elemental analysis instrument techniques typically require destructive and time-consuming specimen preparation, often using concentrated acids or other hazardous materials. Not only is the sample destroyed, waste streams are generated during the analysis process that need to be disposed of, many of which are hazardous.

These aqueous elemental analysis techniques often take twenty minutes to several hours for sample preparation and analysis time. All of these factors lead to a relatively high cost per sample. However, if PPB and lower elemental concentrations are the primary measurement need, aqueous instrument elemental analysis techniques are necessary.

Quantitative elemental analysis for XRF Spectrometry is typically performed using Empirical Methods (calibration curves using standards similar in property to the unknown) or Fundamental Parameters (FP). FP is frequently preferred because it allows elemental analysis to be performed without standards or calibration curves. This enables the analyst to use the system immediately, without having to spend additional time setting up individual calibration curves for the various elements and materials of interest. The capabilities of modern computers allow the use of this no-standard mathematical analysis, FP, accompanied by stored libraries of known materials, to determine not only the elemental composition of an unknown material quickly and easily, but even to identify the unknown material itself.

Scanning Electron Microscope with Energy Dispersive X-Ray Spectrometer (SEM-EDX)

SEM is essentially a high magnification microscope, which uses a focussed scanned electron beam to produce images of the sample, both top-down and, with the necessary sample preparation, cross-sections. The primary electron beam interacts with the sample in a number of key ways:

- Primary electrons generate low energy secondary electrons, which tend to emphasise the topographic nature of the specimen
- Primary electrons can be backscattered which produces images with a high degree of atomic number (Z) contrast

- Ionized atoms can relax by electron shell-to-shell transitions, which lead to either X-ray emission or Auger electron ejection. The X-rays emitted are characteristic of the elements in the top few μm of the sample.

Magnification achievable is about 200,000x to 400,000x magnification. Comparing with optical microscope, SEM also provides much superior depth of field, unflat specimens can still be focused all around. In SEM, we use electron beam to bombard on a sample, which generates secondary electrons (that reveals surface morphology), backscattered electrons (that reveals composition contrast), characteristic Xray (use in elemental analysis), etc. All the signals generated are detected simultaneously by the individual detectors that are currently mounted on Scanning Electron Microscope (SEM)

Typical applications are in materials research, quality control, failure analysis, and forensic science. Industries that commonly use this technique include: semi-conductor and electronics, metals, ceramics, minerals, manufacturing, engineering, nuclear, paper, petroleum, bio-science, and the motor industry.

EDX is the measurement of X-rays emitted during electron bombardment in an electron microscope (SEM or TEM) to determine the chemical composition of materials on the micro and nano- scale. By determining the energies of the X-rays emitted from 80 the area being excited by the electron beam, the elements present in the sample are determined (qualitative analysis). The rate of detection of these characteristic X-rays is used to measure the amounts of elements present (quantitative analysis). If the electron beam is raster over an area of the sample then EDX systems can also acquire X-ray maps showing spatial variation of elements in the sample. It can detect the full range of elements from Boron (atomic no. 5) to Uranium (atomic no. 92).

Particle Size Distribution

Particle size analysis is used to characterize the size distribution of particles in a given sample. Particle size analysis can be applied to solid materials, suspensions, emulsions and even aerosols. There are many different methods employed to measure particle size. Some particle sizing methods can be used for a wide range of samples, but some can only be used for specific applications. It is quite important to select the most suitable method for different samples as different methods can produce quite different results for the same material.

Particle size analysis is a very important test and is used for quality control in many different industries. In just about every industry where milling or grinding is used, particle size is a critical factor in determining the efficiency of manufacturing processes and performance of the final product. Some industries and product types where particle sizing is used includes pharmaceuticals, building materials, paints coatings, food and aerosols.

- Equivalent sphere theory

One basic problem in particle - size analysis is characterizing particles using just one number. Most particle sizing techniques aim report particle size distributions on a two dimensional graph (ie. particle size on the x-axis and quantity of material on the y-axis). However, the difficulty with this is that there is only one shape that can be described by a single unique number, and that is the sphere. Only a sphere measures the same across every dimension. If we say we have a 100 micron sphere, this describes it exactly. We cannot say the same for a cube, where the 100 micron may describe the length of one edge, or even a diagonal transect.

For this reason, all particle sizing techniques measure a one dimensional property of a particle and relate this to the size of an "equivalent sphere". One example

is to measure the surface area of a particle and then report the size of sphere which has the same surface area. Probably the most common method is to measure the "volume" of each particle in a sample and report the size of a sphere which has the same volume as the particles being measured (this is what is done in Laser Diffraction methods).

- Particle Sizing by laser diffraction

Laser diffraction has become one of the most commonly used particle sizing methods, especially for particles in the range of 0.5 to 1000 microns. It works on the principle that when a beam of light (a laser) is scattered by a group of particles, the angle of light scattering is inversely proportional to particle size (ie. the smaller the particle size, the larger the angle of light scattering). Laser diffraction has become very popular because it can be applied to many different sample types, including dry powders, suspensions, emulsions and even aerosols. It is also a very fast, reliable and reproducible technique and can measure over a very wide size range.

Specific Gravity

The density of water is 1 gram/ cm3 which is the same as 1 x 103 kg/m3. The ratio of the density of any solid or liquid or to that of water is called its specific gravity (S). Since it is the ratio of two densities, specific gravity has no units and is independent of the system of measurement. The specific gravity of a liquid can then be measured by finding the ratio of the buoyant force an object feels in the liquid to the buoyant force it feels in water. This is the same as the ratio of the apparent loss of weight in the liquid to the apparent loss of weight in water:

$$S = \frac{w - w_1}{w - w_2}$$

Where w, w1, and w2 represent the object's weight in air, in the liquid, and in water, respectively. Since g is a common factor in the denominator and the numerator it can be factored out and the specific gravity can be written in terms of the object's apparent mass in air, liquid, and water:

$$S = \frac{m - m_1}{m - m_2}$$

VITA

The author of the thesis was born on 2nd May 1987, in Nakhonsrithammarat, Thailand. After receiving her bachelor's degree of engineering on material from the Department of Mining and Material Engineering, Faculty of Engineering, Prince of Songkhla University in 2009, she continuously started her geo-resources engineering master's study, which is presented in this thesis book in the Department of Mining and Petroleum Engineering, Faculty of Engineering, Chulalongkorn University. She was granted friendship JNESYS scholarship to do this thesis during October 2010 - September 2011 from Earth Resources Engineering, Kyushu University, Fukuoka, Japan.